Quarkonia and heavy-quark relaxation times in the quark-gluon plasma

F. Riek* and R. Rapp†
Cyclotron Institute, Texas A&M University, College Station, Texas 77843-3366, USA
(Received 6 May 2010; published 8 September 2010)

A thermodynamic T-matrix approach for elastic two-body interactions is employed to calculate spectral functions of open and hidden heavy-quark systems in the quark-gluon plasma. This enables the evaluation of quarkonium bound-state properties and heavy-quark diffusion on a common basis and thus to obtain mutual constraints. The two-body interaction kernel is approximated within a potential picture for spacelike momentum transfers. An effective field-theoretical model combining color-Coulomb and confining terms is implemented with relativistic corrections and for different color channels. Four pertinent model parameters, characterizing the coupling strengths and screening, are adjusted to reproduce the color-average heavy-quark free energy as computed in thermal lattice QCD. The approach is tested against vacuum spectroscopy in the open (D, B) and hidden (Ψ and Υ) flavor sectors, as well as in the high-energy limit of elastic perturbative QCD scattering. Theoretical uncertainties in the static reduction scheme of the four-dimensional Bethe-Salpeter equation are elucidated. The quarkonium spectral functions are used to calculate Euclidean correlators which are discussed in light of lattice QCD results, while heavy-quark relaxation rates and diffusion coefficients are extracted utilizing a Fokker-Planck equation.

DOI: 10.1103/PhysRevC.82.035201 PACS number(s): 14.40.Pq, 12.38.Mh, 14.40.Lb, 14.40.Nd

I. INTRODUCTION

Hadrons containing heavy quarks are widely used to deduce basic properties of the strong force as given by quantum chromodynamics (QCD) [1]. Heavy-quark (HQ) systems are also valuable for studying hot and dense matter, in particular for temperatures and quark chemical potentials which are parametrically small compared to the HQ mass, $T, \mu_q \ll m_Q$ ($Q = c, b$). Under these conditions, which are believed to encompass phase changes of the medium, HQ momenta ($p_Q^2 \sim m_Q T$) are large relative to those of the (light) partons ($p^2 \sim T^2$) constituting the heat bath. This leads to simplifications in the theoretical description which facilitate the task of studying the medium. For example, the prevalence of elastic interactions with spacelike momentum transfers suggest that a potential picture for HQ interactions—successful in vacuum—may remain valid in the medium.

The modifications of heavy quarkonia (charmonium and bottomonium) in the medium are believed to reveal quark deconfinement in the quark-gluon plasma (QGP) as produced in ultrarelativistic heavy-ion collisions (URHICs; cf. Refs. [2–4] for recent reviews). In addition, open heavy-flavor particles are being utilized to extract transport properties of the medium formed at the Relativistic Heavy Ion Collider (RHIC) by computing their diffusion coefficient in the QGP (see, e.g., Ref. [5] for a recent review). In Ref. [6] it was suggested that the (in-medium) forces responsible for heavy-quarkonium binding may be closely related to those governing the diffusion of an individual heavy quark in the QGP. The basis for this idea is that the exchanged four-momentum, $k = (k_0, \vec{k})$, for the elastic scattering of a (slow) heavy quark is essentially "static," i.e., the energy transfer is parametrically smaller than the three-momentum transfer, $k_0 \simeq \vec{k}^2/2m_Q \ll |\vec{k}|$, for both an individual heavy quark and a quarkonium bound state. A possible consequence of such a connection could be that a "strong" interaction in the medium, which binds charmonium states above the critical temperature, at the same time leads to strong correlations in the heavy-light sector, which accelerate HQ thermalization compared to perturbative scattering [6]. The purpose of the present article is to set up and carry out a framework which enables a systematic investigation of this connection. This requires to evaluate in-medium bound and scattering states on equal footing, which will be realized by employing a thermodynamic T-matrix approach [7,8]. To improve the reliability of this framework, several constraints will be elaborated: input potentials will be adjusted to reproduce the HQ free energy computed in lattice QCD (lQCD) in vacuum and at finite temperature, empirical vacuum spectroscopy in the bound-state regime and perturbative QCD in the high-energy scattering limit will be checked, and Euclidean correlators for heavy quarkonia in medium will be tested with lQCD results.

In the vacuum, the description of heavy quarkonia within a potential framework can be made rigorous as an effective field theory of QCD with heavy quarks, so-called potential nonrelativistic QCD (pNRQCD) [1]. In a hot and dense medium, however, additional scales enter the problem (e.g., temperature, T, and Debye screening mass, m_D) rendering the extension of the potential concept more involved, especially in a strongly interacting system where it is difficult to establish scale hierarchies (for perturbative treatments based on $T \gg m_D \sim gT$, see, e.g., Refs. [9–11]). On the other hand, nonperturbative information on the HQ interaction over a wide range of temperatures is available from thermal lQCD in terms of the free energy, F, of a static $Q\bar{Q}$ pair (strictly speaking, the difference in free energy of the system with and without the HQ pair) [12–14]. In practical approaches,

*friek@comp.tamu.edu
†rapp@comp.tamu.edu

the color-singlet free energy, F_1 (or the pertinent internal energy, $U_1 = F_1 - T\,\partial F_1/\partial T$) has been utilized as a potential in Schrödinger [15–18] and T-matrix [7,8] equations, and the resulting spectral functions have been checked against lQCD results for Euclidean correlation functions. While these approaches suggest that the potential model provides a viable tool at finite temperature, several open issues remain, e.g.: (i) the use of free or internal energy (or even combinations thereof [19]); (ii) the gauge dependence of the color-singlet free energy [20]; (iii) microscopic insights into the screening mechanisms (e.g., color-Coulomb vs. confining forces); and (iv) corrections to (or even validity of) the potential ansatz. In the present article we do not offer new principle insights on item (i). To cover the uncertainty associated with this problem, our calculations will be carried out for both free and internal energies which are believed to bracket the limiting cases within their interpretation as a finite-temperature HQ potential. To address items (ii) and (iii) we adopt a recently proposed field-theoretic ansatz [21,22] to describe HQ free energies using a screened Coulomb plus "confining" gluon propagator. These propagators require four input parameters (coupling strengths and screening masses) which are adjusted to reproduce gauge-invariant color-average free energies from lQCD. Color projections are extracted within the model and utilized to compute color-singlet quarkonium and heavy-light spectral functions, as well as colored correlations which contribute to the transport of heavy quarks in the QGP. As for item (iv), special care is taken of relativistic effects—especially for light quarks—which in our framework is possible once the vector and/or scalar nature of the Coulomb and confining force is specified. For example, the relativistic Breit correction known from electrodynamics [23] naturally emerges as a relativistic effect in the Coulomb potential. We will furthermore check the static approximation underlying the potential picture by comparing different versions of the three-dimensional reduction scheme to obtain the T matrix from an underlying Bethe-Salpeter equation.

This article is organized as follows. In Sec. II we set up the microscopic model used to fit lQCD free energies. In Sec. III we recollect main elements of the thermodynamic T-matrix formalism, including relativistic corrections. Section IV is devoted to the discussion of our numerical results for quarkonium and heavy-light spectral functions and their applications to Euclidean correlators and HQ relaxation times, respectively. We conclude in Sec. V.

II. MICROSCOPIC MODEL FOR THE HEAVY-QUARK POTENTIAL

The recent revival of potential models to describe heavy quarkonia in medium has been largely driven by the prospect of a paremeter-free input via static HQ free energies computed in thermal lQCD. However, functional fits to the lattice "data" usually do not offer much insight into the physical mechanisms underlying the medium effects in the potential nor do they allow to define vertex structures of the interaction which become important at higher energies and/or in different color channels. In addition, it is desirable to base the starting point on a gauge-invariant quantity, i.e., the color-average free energy.[1] To this end, we adopt the microscopic model developed by Megías *et al.* [21,22] which we briefly review in the following and then fit to lattice data. The key idea underlying this model is that the HQ free energy can be accounted for by a nonperturbative ansatz for the gluon propagator giving rise to a stringlike confining term in coordinate space, plus a "standard" perturbative term corresponding to a screened color-Coulomb interaction [21],

$$\begin{aligned} D_{00}(\vec{k}) &= D_{00}^{P}(\vec{k}) + D_{00}^{NP}(\vec{k}) \\ D_{00}^{P}(\vec{k}) &= \frac{1}{\vec{k}^2 + m_D^2} \qquad D_{00}^{NP}(\vec{k}) = \frac{m_G^2}{\left(\vec{k}^2 + \tilde{m}_D^2\right)^2} \end{aligned} \tag{1}$$

to be understood in static gauge and within dimensional reduction ($m_D, \tilde{m}_D$: screening masses). The leading nonperturbative effect in the gluon propagator is associated with a dimension-2 gluon condensate dictated by dimensional considerations,

$$\left\langle A_{0,a}^2 \right\rangle^{NP} = T\,\frac{\left(N_c^2 - 1\right) m_G^2}{8\pi \tilde{m}_D}, \tag{2}$$

with m_G^2 a "glueball" mass. *A priori*, a dimension-2 gluon condensate is gauge dependent and as such a somewhat controversial quantity. Since the gluon propagator is a gauge-dependent quantity the appearance of gauge-dependent terms is inevitable. However, it has been argued by several authors [24–28] that a dimension-2 condensate encodes nontrivial gauge-invariant information, e.g., topological configurations associated with magnetic monopoles giving rise to a static confining force (which is precisely the effect modeled in the present context). Evidence for a dimension-2 condensate contribution has also been found in QCD sum rules (see Ref. [29] and references therein).

To establish the connection to the HQ free energy (given by a correlator of Polyakov loops, Ω), one starts from its perturbative expression at finite temperature in the color-singlet channel [21],

$$\begin{aligned} e^{-F_1(r,T)/T} &= \left\langle \frac{1}{N_c} Tr[\Omega(x)\Omega^{\dagger}(y)] \right\rangle \\ &= e^{(g^2/(2N_c T^2))\,\langle A_{0,a}(x) A_{0,a}(y) - A_{0,a}^2(x)\rangle} + \mathcal{O}(g^6), \end{aligned} \tag{3}$$

with the perturbative gluon propagator

$$\langle A_{0,a}(x) A_{0,b}(y)\rangle = \delta_{ab} T \int \frac{d^3k}{(2\pi)^3} e^{i\vec{k}\cdot(\vec{x}-\vec{y})} D_{00}^{P}(\vec{k}). \tag{4}$$

The separation-independent term, $\langle A_{0,a}^2(x)\rangle$, in Eq. (3) plays the role of a self-energy of an individual heavy quark. The main assumption consists now of augmenting the perturbative propagator by the nonperturbative one as given by Eq. (1). Assuming further that the same functional dependence as in Eq. (3) holds in the nonperturbative case we are lead to the

[1] Since the model adopted here and the lattice calculations use different gauges (static vs. Coulomb), this is the only meaningful way to extract parameters.

following form of the singlet free energy ($N_c = 3$):

$$F_1(r,T) = -\frac{4}{3}\alpha_s\left(\frac{1}{r}e^{-m_D r} + \frac{m_G^2}{2\tilde{m}_D}e^{-\tilde{m}_D r} - \frac{m_G^2}{2\tilde{m}_D} + m_D\right). \tag{5}$$

In Ref. [21] this approach has been applied to study the Wilson loop and HQ free energy in quenched QCD at finite temperature and efficiently reproduces pertinent lQCD data. As an extension of this treatment we allow for different screening masses in the perturbative and nonperturbative parts of the gluon propagator which improves the precision in our fits to unquenched lQCD data. As indicated above we fit the color-average free energy. Since we aim at a parametrization over a large range in distance and temperature we employ the definition [30]

$$F_{av}(r,T) = -T\,\ln\left[\tfrac{1}{9}e^{-F_1(r,T)/T} + \tfrac{8}{9}e^{-F_8(r,T)/T}\right] \tag{6}$$

without further approximations which automatically ensures the correct behavior in the limits $rT \gg 1$, where the potential is dominated by two-gluon exchange, $F_{\rm av}(r,T) \approx [F_1(r,T)]^2$, and $rT \ll 1$, where we have $F_{\rm av}(r,T) \approx F_1(r,T) + T\ln(9)$ [31]. The evaluation of Eq. (6) requires the color-octet and -singlet free energies (in addition we will use the extracted potentials in the sextet and antitriplet channels for the calculation of HQ relaxation times). In previous works [6,8] these potentials have been approximated by Casimir scaling of the singlet potential. While this is a good approximation for the short-range (perturbative/Coulombic) part of the potential [31,32], it presumably does not apply to the confining part which rather appears to be universal, including its long-distance limit [30,33,34].[2] We therefore apply Casimir scaling only to the Coulomb part of the model gluon propagator while the string part is assumed to be color-blind, i.e., the same in all color channels.[3]

This is also compatible with the interpretation of the long-distance limit as an individual HQ self-energy, as discussed below. The coordinate-space potential in a color channel a takes the form

$$\begin{aligned} F_a(r,T) &= -\frac{4}{3}\alpha_s\left(\frac{C_a}{r}e^{-m_D r} + \frac{m_G^2}{2\tilde{m}_D}e^{-\tilde{m}_D r} - \frac{m_G^2}{2\tilde{m}_D} + m_D\right) \\ &\equiv F_a^C(r,T) + F^S(r,T) + F_\infty(T) \qquad (7) \\ C_1 = 1 \quad C_8 = -1/8 \quad C_6 = -1/4 \quad C_{\bar{3}} &= 1/2, \end{aligned}$$

with the Coulomb part F_a^C, the nonperturbative string part F^S, and an r-independent part, $F_\infty(T)$, which will be associated with a (real part of the) HQ "self-energy," Σ_Q^R, below. Similar analytic forms of the potential have been used for fits to the color-singlet potential in Ref. [18]. Let us examine two limits of this expression. First, for $T \to 0$ both screening masses should vanish while the condensate characterized by m_G remains finite [21]; one obtains [21]

$$F_a(r,T=0) = -\frac{4}{3}\alpha_s\frac{C_a}{r} + \sigma\, r, \quad \sigma = \frac{2\,\alpha_s\, m_G^2}{3}, \tag{8}$$

which recovers the Cornell potential in the color-singlet channel and yields a universal string tension in all color channels, consistent with Refs. [30,33,34]. Second, for $r \to \infty$ at finite T one has

$$F_\infty \equiv F_a(r\to\infty,T) = \frac{4}{3}\alpha_s\left(-m_D + \frac{m_G^2}{2\tilde{m}_D}\right), \tag{9}$$

which is independent of a, consistent with lQCD data in Refs. [14,30]. When additionally taking the zero-temperature limit of F_∞, it diverges since $m_G > 0$ and $\tilde{m}_D \to 0$. This is, of course, expected in quenched QCD but needs to be amended in the presence of light quarks, to simulate "string breaking." We implement this by enforcing a flat potential above a string-breaking scale of about $r \simeq 1.1$ fm where the potential has reached about 1.1 GeV. We now also see that the cancellation between the leading piece of the second term and the constant third term in the parentheses of Eq. (7) in the $\tilde{m}_D \to 0$ limit works only for all color channels if the string term is color-blind (i.e., has no Casimir scaling). If, on the other hand, both terms proportional to m_G^2 are subject to Casimir scaling, it would imply that the $r \to \infty$ limit (i.e., the single HQ self-energy) picks up a strong dependence on the color orientation of the quark, which is not natural.

Once the temperature dependence of the parameters m_G, m_D, and $\tilde{m}_D$, as well as of the strong coupling, α_s, is determined through fits of the color-average free energy, corresponding expressions for the internal energy, U, can be computed via

$$U(r,T) = F(r,T) - T\frac{d}{dT}F(r,T) \tag{10}$$

and projected into different color channels, a.

It is currently an unsettled question whether the free or internal energy (or a linear combination thereof) is a more suitable quantity to be utilized as a static two-body potential in a Schrödinger and/or scattering equation. We recall that the quantity, $F(r,T)$, computed in thermal lQCD, is the difference between the free energies of the thermal system containing a static $Q\bar{Q}$ pair and the thermal system without the pair. In Ref. [36] it has been argued that the pertinent difference in internal energies, $U(r,T)$, recovers the thermal expectation value of the potential energy between the static Q and $\bar{Q}$ charges. This suggests $U(r)$ as the appropriate in-medium two-body potential. Such a potential would by construction be a real quantity and thus a natural starting point to be unitarized in a scattering equation, generating appropriate on-shell cuts in the intermediate state through imaginary parts in the scattering amplitude. In Ref. [37] it has been argued that the relevance of F vs. U depends on the interplay of the thermal relaxation time in the heat bath and the interaction time of the Q and $\bar{Q}$. If the former is much shorter than the latter, the $Q\bar{Q}$ motion will be adiabatic and the free energy should be used; on the other hand, for very short interaction times (e.g., for a broad resonance or high-energy scattering),

[2] Calculations reported in Ref. [35] come to a different conclusion, possibly because they cover smaller distances than those in Refs. [30,34]. In Ref. [30] potential problems with the computation of the octet free energy on the lattice below T_c have been pointed out.

[3] Such a decomposition is not possible in functional parametrizations of the potential.

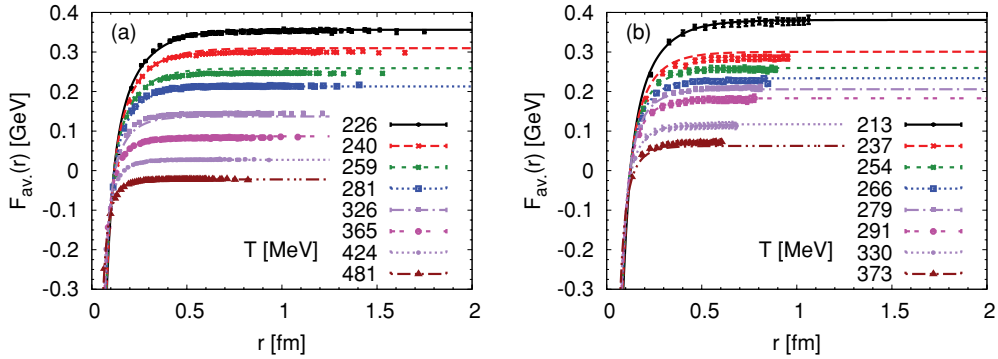

FIG. 1. (Color online) Color-average HQ free energies obtained in thermal lQCD computations by Kaczmarek *et al.* (left panel) [12,39] and Petreczky *et al.* (right panel) [13,41] compared to our fits using the microscopic model suggested in Refs. [21,22].

the internal energy should be more suitable. Another approach to the problem has been pursued by using effective field theories at finite temperature [9,11] by combining HQ and perturbative hierarchies (HQ speed $v \ll 1$ and $gT \ll T$). These studies recover the color-Coulomb part of the interaction and suggest that the free energy plays the role of a potential in a Schrödinger equation. In addition, an imaginary part of the effective potential has been identified [10,38]. We emphasize, however, that within a T-matrix approach, imaginary parts are generated via the unitarization procedure in the intermediate propagator and thus imaginary parts in the potential should be implemented via suitable cuts in a coupled-channels treatment. To account for the present uncertainty in the identification of an irreducible two-body HQ potential we will show numerical results for both F and U as driving kernel in the T-matrix equation. More precisely, we utilize the subtracted quantity

$$V_a(r;T) = X_a(r,T) - X(r \to \infty, T), \quad X = F \text{ or } U \qquad (11)$$

to ensure convergence of the Fourier transform. These choices are believed to bracket the range of interaction strength in the HQ sector.

In addition to the potential, another important ingredient to the two-body scattering equation are the in-medium self-energies of the heavy quark and antiquark, which we treat symmetrically as appropriate for a hot medium at vanishing baryon chemical potential. Starting from a bare quark of mass m_Q^0, we interpret the potential value at infinite distance, $X(r \to \infty, T)$ in Eq. (11), as a temperature-dependent "mean-field" contribution to the HQ masses, i.e., as a real part of the self-energy,

$$m_Q = m_Q^0 + \Sigma_Q^R(T), \quad \Sigma_Q^R(T) \equiv X(r \to \infty, T)/2. \qquad (12)$$

This interpretation follows from the picture that at infinite distance the quarks have become independent of each other which is supported by lQCD results as discussed above. In addition, we will investigate the effects of imaginary parts of the HQ self-energy,

$$\Gamma_Q = -2 \,\mathrm{Im}\, \Sigma_Q, \qquad (13)$$

associated with HQ rescattering in the heat bath. This quantity has been estimated to be about ~0.2 GeV in the T-matrix calculations of Ref. [6].

Let us now turn to the fit of the potentials to recent lQCD data for the color-average free energy. To obtain an indication of the systematic uncertainty underlying different lQCD inputs we will carry out all our calculations for $N_f = 2+1$-flavor QCD [12,39,40] and for $N_f = 3$-flavor QCD [13,41] (the latter input has been used in the color-singlet channel in a previous T-matrix study [7]), which we refer to in the following as potentials 1 and 2, respectively. The underlying (pseudo-) critical temperatures in these lQCD calculations have been quoted as $T_c = 196$ MeV (potential 1) and 190 MeV (potential 2). Figure 1 shows the pertinent color-average free energies together with our fits which have been performed down to temperatures of ca. 0.8 T_c (not all are shown in the plot). The agreement with each data set is fair and supports the adequacy of the underlying model. The temperature dependence of the four fit parameters is displayed in Fig. 2. The variation of all parameters between the two potentials is rather small. The strong coupling constant, $\alpha_s(T)$, depends weakly on T. To suppress fluctuations in an unconstrained fit, we have, for simplicity, adopted a linear ansatz.[4] The screening masses exhibit an appreciable increase with temperature reminiscent of the linear T dependence one expects from leading-order perturbation theory, $m_D^{\text{pert}} = (1 + N_f/6)^{1/2} gT$. Compared to the perturbative result, the coefficients in our fits are smaller for the Coulomb part (m_D) and larger for the "string" part ($\tilde{m}_D$), suggesting a stronger screening of the confining part (which primarily acts at larger distances). We have tried fits enforcing the condition $m_D = \tilde{m}_D$ but could not obtain satisfactory accuracy without introducing unnaturally large variations of the parameters. This might support the assertion of differences in the screening process for the perturbative and nonperturbative components of the free energy. On the other hand, the variation of the glueball mass with T is weak. Recalling the explicit relation to the dimension-2

[4]Without this constraint, the fits tend to generate what we believe are artificially large variations in the parameters, mainly caused by varying ranges in r as covered by the lQCD data at different temperatures. This is particularly evident when fitting to the color-singlet free energy and removing some of the small-distance points. As a general guiding principle in the fits we tried to utilize redundancies in parameter choices to obtain smooth variations with T.

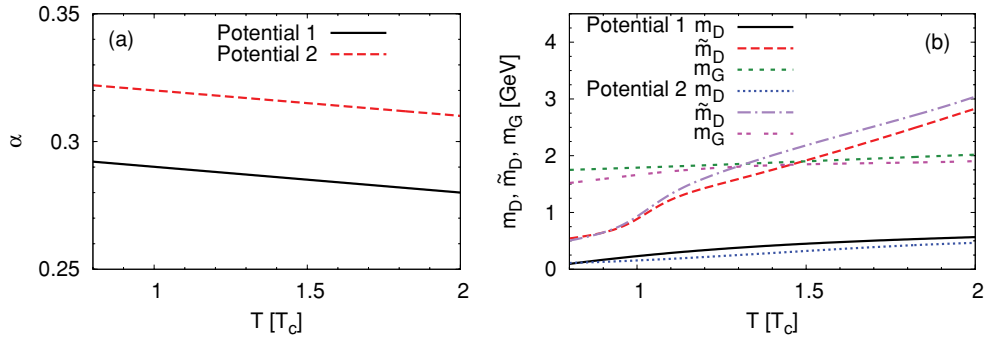

FIG. 2. (Color online) Temperature dependence of the parameters deduced from our fit to the color-average free energies from the two lQCD calculations displayed in Fig. 1. (Left panel) Strong coupling constant α_s; (right panel) screening masses of the color-Coulomb and confining parts, and dimension-2 condensate "glueball mass," m_G.

condensate [21]

$$C_2 = g^2\langle A^2_{0,a}\rangle^{NP} = 4\alpha_s\, T\, \frac{m_G^2}{\tilde{m}_D}\,, \tag{14}$$

we find that a constant of about $C_2 \simeq 0.8$ GeV^2 above T_c (see left panel of Fig. 3) is well compatible with our fit, as also found previously in Ref. [21] and in analyses of the gluon propagator, three-gluon vertex or quark propagator (see Ref. [22] and references therein). On the other hand, we have verified that the 20% decrease of $C_2(T)$ across T_c is a robust feature within "reasonable" variations of the other fit parameters; e.g., when imposing an overall T-independent value for C_2, we could not reproduce the lQCD values of $F_{\rm av}^{\infty}$ over the entire temperature range without "unnaturally" large variations in the other fit parameters. It is tempting to speculate that the 20% drop in $C_2(T)$ across T_c is related to a similar drop found in the magnetic-monopole density in SU(2) gluodynamics in Ref. [25], where qualitative arguments have been put forward that an A^2_μ condensate could be connected to the monopole density. The temperature window over which the variation of $C_2(T)$ occurs basically conicides with where rapid changes in the infinite-distance values F_∞ and U_∞ are observed, cf. the right panel of Fig. 3. In the zero-temperature limit, assuming that both screening masses go to zero, a value of $m_G \approx 1$ GeV is needed to reproduce the vacuum string tension of $\sqrt{\sigma} = 0.465$ GeV found in lQCD [39,41], in connection with strong couplings of $\alpha_s = 0.285$ and 0.33 for potentials 1 and 2, respectively. All of these values are close to the fitted ones at the lowest temperature.

In Fig. 4 we summarize the results for the vacuum potentials in the four different color channels which can be formed in two-body $Q\bar{Q}$ and QQ systems [recall that in vacuum the entropy-term vanishes and thus $F_a = U_a$; also $F_{\rm av} = F_1$ from Eq. (6)]. The color blindness of the string term produces a long-range attraction in all channels (which will support colored bound states in vacuum as discussed in Sec. IV A). The potentials emerging from the model-fit at finite T are collected in Fig. 5. One clearly recognizes the "melting" of the string term with increasing T. The singlet (meson) and antitriplet (diquark) potentials remain attractive at all distances. For the octet and sextet potential some residual attraction from the string term persist at lower temperatures (especially in U), preserving a shallow dip structure for quark separations of around 0.1–0.2 fm. This behavior has also be seen on the lattice [14] and is obviously incompatible with a Casimir scaling of the string term.

III. THERMODYNAMIC T MATRIX AND OBSERVABLES

A. Reduction scheme and relativistic corrections

The above constructed in-medium potentials are now implemented into a thermodynamic T-matrix approach. The latter follows from a three-dimensional (3D) reduction of

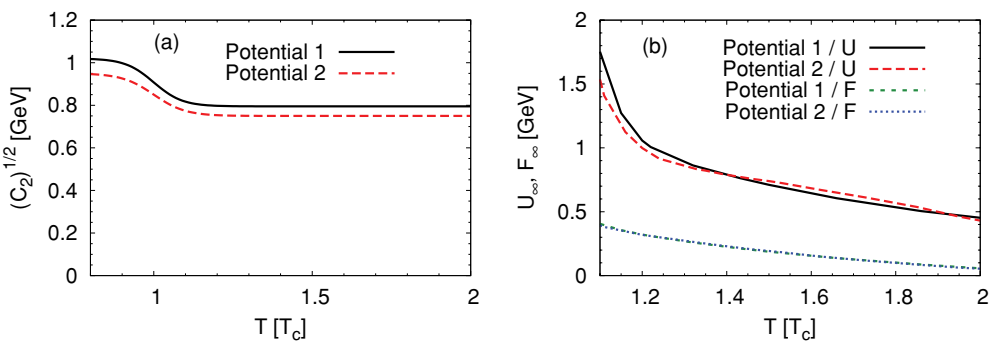

FIG. 3. (Color online) Temperature dependence of the dimension-2 condensate C_2, Eq. (14), (left panel) and of the infinite-distance limit of the free and internal energies for the two lQCD computations displayed in Fig. 1.

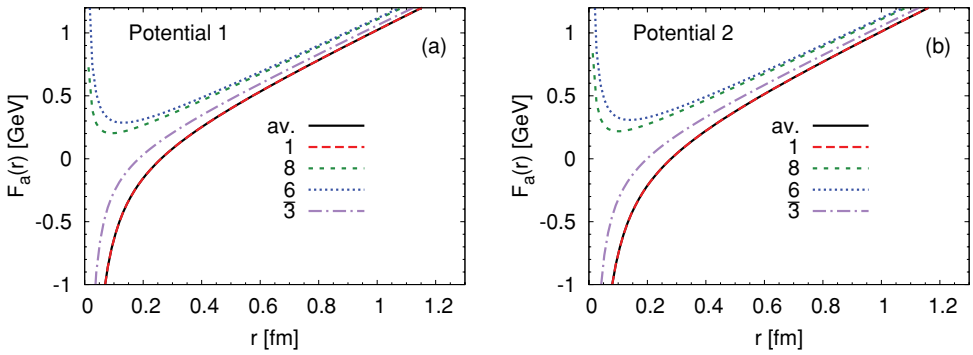

FIG. 4. (Color online) Vacuum HQ potentials in different color configurations of $Q\bar{Q}$ (singlet and octet) and QQ (triplet and sextet) channels, extracted from model-fits to color-average $Q\bar{Q}$ free energies in lQCD for $N_f = 2+1$ [12,39,40] ("potential 1," left panel) and for $N_f = 3$ [13,41] ("potential 2," right panel).

the Bethe-Salpeter equation in ladder approximation [42–44]. Heavy-quark systems are particularly suitable for this reduction as their energy transfer is parametrically suppressed compared to the momentum transfer. Even for heavy-light systems the on-shell condition on the heavy quark suppresses the energy transfer relative to the three-momentum transfer. Note that a 4D treatment cannot improve the accuracy as long as the input is based on static potentials. However, relativistic corrections, as well as different reduction schemes, should and will be addressed below. The former are necessary to ensure

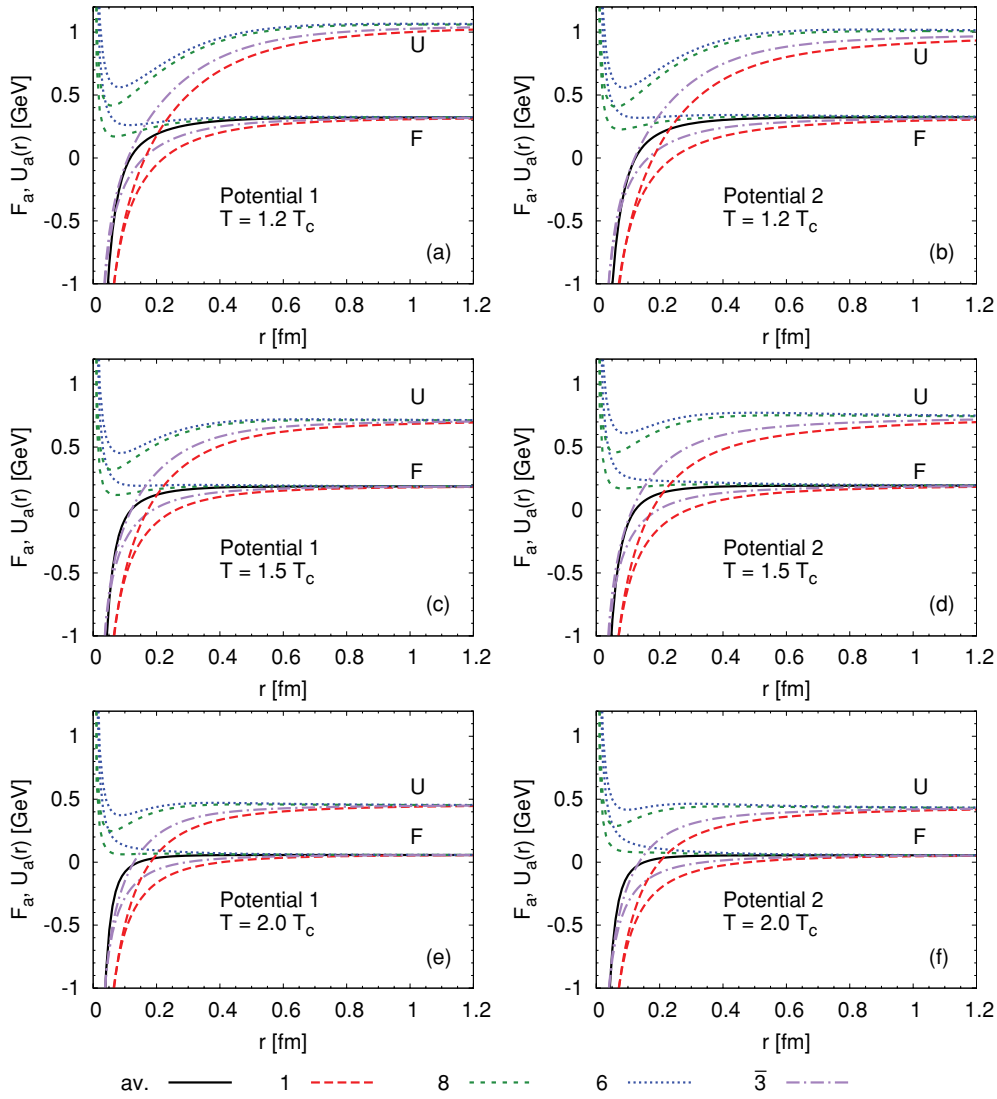

FIG. 5. (Color online) In-medium heavy-quark free and internal energies at various temperatures in color-singlet (long-dashed lines), -octet (short-dashed lines), -anti-triplet (dash-dotted lines), -sextet (dotted lines), and -average (solid lines) channels, extracted from $N_f = 2+1$ (left column) and $N_f = 3$ lQCD computations (right column).

consistency for relativistic energies (and, in fact, establish "minimal" Poincaré invariance of the potential approach [45]; see also Ref. [46]), while the latter give an indication of uncertainties inherent in the static approximation. The 3D integral equation for the T matrix can be further simplified by applying a partial-wave decomposition which leads to the following 1D equation,

$$\begin{aligned} &T_{l,a}(E;q',q) \\ &\quad = \mathcal{V}_{l,a}(q',q) + \frac{2}{\pi}\int_0^\infty dk\, k^2\, \mathcal{V}_{l,a}(q',k) \\ &\qquad \times G_{12}(E;k)\, T_{l,a}(E;k,q)\,\{1 - n_F[\omega_1(k)] - n_F[\omega_2(k)]\}, \end{aligned} \tag{15}$$

for the T-matrix $T_{l,a}$ in a given color channel (a) and partial wave (l); n_F is the Fermi-Dirac distribution, and $q = |\vec{q}\,|$, $q' = |\vec{q}\,'|$, and $k = |\vec{k}\,|$ denote the relative three-momentum moduli of the initial, final, and intermediate two-particle state, respectively, and $\omega_i(k) = (m_i^2 + k^2)^{1/2}$ the single-quark energies. Equation (15) encompasses both the heavy-light ($1 = Q$, $2 = q$) and quarkonium ($1, 2 = Q$) channels where either particle can be a quark or an antiquark. The precise form of the two-particle propagator, G_{12}, depends on the reduction scheme [47,48], for which we will investigate two well-established options, namely the Blancenbecler-Sugar (BbS) [42] and the Thompson (Th) [43] scheme,

$$\begin{aligned} G_{12}^{\rm Th}(E;q) &= \frac{m(q)}{E - \omega^q(q) - \omega^Q(q) - \Sigma_q - \Sigma_Q}, \\ G_{12}^{\rm BbS}(E;q) &= \frac{2\,m(q)\,(\omega^q(q) + \omega^Q(q))}{E^2 - [\omega^q(q) + \omega^Q(q) + \Sigma_q + \Sigma_Q]^2}, \\ m(q) &= \frac{m_q\, m_Q}{\omega^q(q)\,\omega^Q(q)}. \end{aligned} \tag{16}$$

The main difference between both schemes is that the dependence on the total energy, E, is quadratic for the BbS propagator but linear for the Thompson version. The form of the propagators in Eqs. (16) further implies that both quarks remain good quasiparticles in the medium, i.e., their widths $\Gamma_{Q,q}$ are small compared to their mass. We use a minimal width of $\Gamma_{q,Q} = 20$ MeV to facilitate numerical stability, unless otherwise stated. The incorporation of microscopic quark spectral functions will be carried out in an upcoming study. Once the potential is specified, the T-matrix equation (15) is solved using the algorithm of Haftel and Tabakin [49] as in previous works in our context [7,8].

It remains to specify how we implement the coordinate-space potential as extracted from lQCD in the previous section. We start by performing the Fourier transform and partial-wave expansion according to

$$\begin{aligned} V_{l,a}^{C/S}(q',q) &= \int \frac{d^3r\, dx_{q'q}}{8\pi}\, P_l(x_{q'q}) V_a^{C/S}(r) e^{i(\vec{q}-\vec{q}\,')\vec{r}} \\ x_{q'q} &= \frac{\vec{q}\,'\cdot\vec{q}}{\sqrt{|\vec{q}\,'|\,|\vec{q}|}} \end{aligned} \tag{17}$$

with the usual Legendre polynomials P_l. Since the string part of the potential (V^S) is primarily active at long distances, i.e., at low momenta and thus in the nonrelativistic regime, no further amendments are applied to it. However, for the Coulomb part (V^C), which dominates at small distances (and thus at relatively large momentum transfers), several corrections are in order. To infer relativistic effects, let us back up to the definition of the relativistic Coulomb potential given by the perturbative one-gluon exchange diagram in Fig. 6.

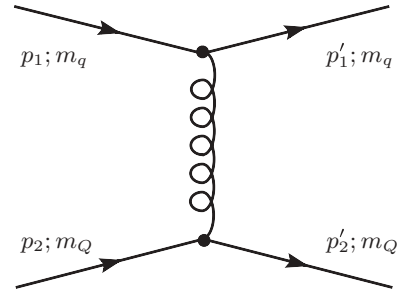

FIG. 6. One-gluon exchange diagram for quark-quark scattering; in the center-of-mass system, the relative four-momentum in the incoming (outgoing) state is $q = (p_1 - p_2)/2$ [$q' = (p_1' - p_2')/2$].

Suppressing the color structure, the Born amplitude (potential) is given by

$$V \sim \underbrace{\frac{4\pi\alpha_s}{t - m_D^2}}_{\text{Yukawa}}\ \underbrace{\bar{u}(p_1')\,\gamma^\mu\,u(p_1)\,\bar{u}(p_2')\,\gamma_\mu\,u(p_2)}_{\text{Spinor-contraction}} \tag{18}$$

where we have included a Debye mass as the leading temperature correction in the gluon propagator. In addition to the standard Yukawa propagator [which in the static approximation amounts to setting $t \to -(\vec{q} - \vec{q}\,')^2$ in the center of mass system] we have a contribution from the contraction of the spinors with the vertex. At the level of the cross section (or amplitude squared) this part gives rise to the following factor (with the normalization $\bar{u}\,u = 1$),

$$\begin{aligned} &|\bar{u}(p_1')\,\gamma^\mu\,u(p_1)\,\bar{u}(p_2')\,\gamma_\mu\,u(p_2)|^2 \\ &\quad = \frac{8\big[2\big(s - m_q^2 - m_Q^2\big)^2 + 2\,s\,t + t^2\big]}{16\,m_q^2\,m_Q^2}. \end{aligned} \tag{19}$$

For large $s = E^2$ the terms proportional t are subleading and can be dropped so that we can reformulate this expression as

$$\begin{aligned} &|\bar{u}(p_1')\,\gamma^\mu\,u(p_1)\,\bar{u}(p_2')\,\gamma_\mu\,u(p_2)|^2 \\ &\quad \simeq \frac{8\big[2\big(s - m_q^2 - m_Q^2\big)^2\big]}{16\,m_q^2\,m_Q^2} = 4\frac{\omega_q^2\,\omega_Q^2}{m_q^2\,m_Q^2}\left(1 + \frac{q^2}{\omega_q\,\omega_Q}\right)^2. \end{aligned} \tag{20}$$

The factor in parenthesis is precisely the well-known Breit interaction in electrodynamics, corresponding to a magnetic current-current interaction of two moving charges [23,37,50], while the first factor "corrects" for relativistic kinematics (the extra factor 4 arises from the summation over spins and has to be taken out in a spin-independent definition of the potential). We therefore identify the following factors with which the nonrelativistic (off-shell) potential, $V(q,q')$, should

be augmented:

$$R(q',q) = m(q)^{-1/2}\, m(q')^{-1/2} \tag{21}$$

$$B(q',q) = b(q)^{1/2}\, b(q')^{1/2} \tag{22}$$

$$b(q) = \left[1 + \frac{q^2}{\omega_q(q)\,\omega_Q(q)}\right]. \tag{23}$$

Note that $B, R \to 1$ for $q, q' \ll m_{Q,q}$. For the string term, for which we assume a scalar interaction, the spinor contraction leads to

$$|\bar{u}(q')\, u(q)\, \bar{u}(p')\, u(p)|^2 = \frac{4\left(4\,m_q^2 - t\right)\left(4\,m_Q^2 - t\right)}{16\,m_q^2\, m_Q^2}. \tag{24}$$

Assuming again that we can drop the terms proportional t (relative to $m_{Q,q}$), no relativistic correction factor is mandated (this refines the procedure adopted in earlier works [7,8]).

To check the impact of our corrections we compute the cross sections for one-gluon exchange (Fig. 6) for quark-quark scattering using the Coulomb term in Born approximation including our correction factors,

$$\frac{d\sigma}{d\Omega} = \frac{1}{64\pi s}\,\frac{2}{36}\,\frac{m_q^2\, m_Q^2}{\omega_q^2\,\omega_Q^2}\sum_{l,a}|T_{l,a}|^2, \quad T_{l,a} = \mathcal{V}_{l,a}^C, \tag{25}$$

and compare it to the exact perturbative QCD (pQCD) results in the left panel of Fig. 7. One finds that the relativistic correction factors B and R are essential to establish consistency with pQCD at high energies; even at low energies, the agreement is no worse than 20%, which supports the approximation of neglecting t against s and $m_{Q,q}$ in the numerator of Eq. (19). The factors R and B provide a substantial improvement over not including them. Without the R factor, one obtains vanishing cross sections at high energy (only half of the correct magnitude without the Breit correction); even close to threshold the discrepancy to pQCD is larger than with the corrections. Also note that without the relativistic factors the cross section goes to zero for $m_q \to 0$, which becomes an uncontrolled feature in applications to heavy-light scattering. In the right panel of Fig. 7 we compare a pQCD calculation assuming a scalar vertex structure to the T-matrix Born results with and without correction factors B and R. In this case, it is obviously mandated not to include these factors. As to be expected, the nonrelativistic approximation leads to the same result irrespective of whether one uses a vector or scalar interaction.

Finally, we account for effects of the running coupling constant in the off-shell extrapolation of the potential. For on-shell kinematics, $q = q'$, such effects are effectively taken care of by our parametrization of the potential. For off-shell scattering, we simulate the running coupling by introducing a factor $F_{\rm run}(q \neq q') < 1$ as

$$F_{\rm run}(q',q) = \ln\left[\frac{\Delta^2}{\Lambda^2}\right] \Big/ \ln\left[\frac{(q-q')^2 + \Delta^2}{\Lambda^2}\right] \tag{26}$$

with $\Delta = 1$ GeV and $\Lambda = 0.2$ GeV.

Putting all corrections together, the final form of the potential figuring in the T-matrix equation (15) is

$$\mathcal{V}_{l,a}(q',q) = R(q',q)\, B(q',q)\, F_{\rm run}(q',q)\, V_{l,a}^C(q',q) + V_{l,a}^S(q',q). \tag{27}$$

In vacuum the unscreened Coulomb potential exhibits a well-known infrared singularity. We tame this by introducing a small low-momentum cutoff; we have checked that varying this cutoff has a very small effect on the vacuum spectral functions.

B. Quarkonium correlators and HQ diffusion

The key quantity for computing observables is the on-shell T-matrix, $T_{l,a}(E;q,q)$, where $E = \omega_1(q) + \omega_2(q)$ for both in- and outgoing channels. Following Ref. [7], the continuation below the two-particle threshold, $E_{\rm thr} = m_1 + m_2$, is carried out for vanishing three-momentum, $T_{l,a}(E;0,0)$. The mesonic spectral function in a given quantum-number channel α is defined as

$$\sigma_\alpha(E) = -\frac{1}{\pi}\,{\rm Im}\,\mathcal{G}_\alpha(E), \tag{28}$$

where $\mathcal{G}$ denotes the correlation function, for which we will focus on the case of a heavy quark and antiquark ($Q\bar{Q}$) in the color-singlet channel ($a = 1$) in a QGP of vanishing net

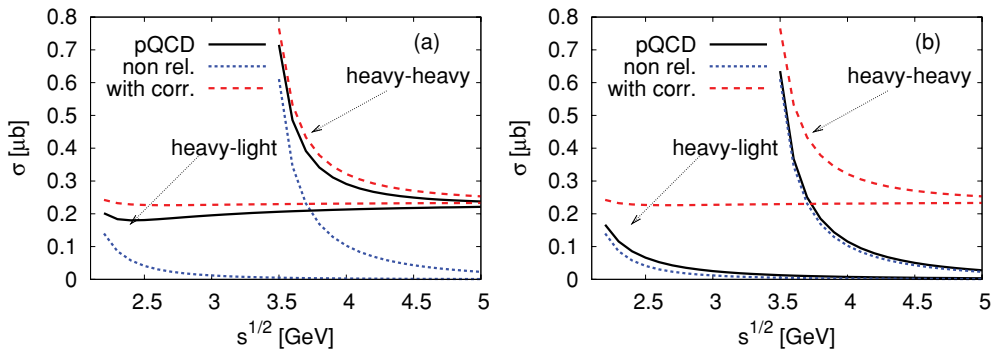

FIG. 7. (Color online) (Left panel) Perturbative QCD cross section for quark-quark scattering via t-channel gluon exchange using a vector interaction. The full pQCD result (solid line) is compared to the T-matrix result in Born approximation using (i) a nonrelativistic treatment of the spinor structure (doted line) and (ii) the correction factors R and B. (Right panel) The same but for a scalar interaction. The heavy- and light-quark masses are set to 1.7 and 0.4 GeV, respectively, and the strong coupling and Debye mass have been fixed at 0.3 and 0.67 GeV, respectively.

baryon charge (μ_q). It can be written as

$$\mathcal{G}_\alpha(E) = \mathcal{G}^0_\alpha(E) + \Delta\mathcal{G}_a(E), \tag{29}$$

where

$$\mathcal{G}^0_\alpha(E) = i N_f N_c \int \frac{d^3k}{(2\pi)^3} G_{12}(E;k)\,[1 - 2n_F(\omega_Q(k)] \times \mathrm{Tr}[\Gamma_\alpha\, \Lambda_+(\vec{k}\,)\,\Gamma_\alpha\, \Lambda_-(-\vec{k}\,)] \tag{30}$$

denotes the noninteracting contribution with the particle/antiparticle projectors

$$\Lambda_\pm(\vec{k}\,) = \frac{\omega_Q(k)\gamma^0 - \vec{k}\cdot\vec{\gamma} \pm m_Q}{2\,m_Q}. \tag{31}$$

The Dirac matrices $\Gamma_\alpha \in \{1, \gamma_\mu, \gamma_5, \gamma_\mu\gamma_5\}$ characterize the scalar, vector, pseudoscalar, and pseudovector channels, respectively (corresponding to χ_{c0}, J/ψ, η_c, and χ_{c1} in the charmonium sector). In the following we will neglect effects due to spin-orbit and spin-spin (hyperfine) interactions which is justified in the HQ limit. It implies degeneracy of the S-wave ($l = 0$) states J/ψ and η_c, as well as of the P-wave ($l = 1$) χ_c states (in the vacuum spectrum, this is realized within $\sim$0.1 GeV). Thus, we will compute only the vector ($\Gamma_\alpha = \gamma_\mu$) and scalar ($\Gamma_\alpha = 1$) channels. The interacting contribution to the correlator in Eq. (29) is given in terms of the off-shell T matrix as

$$\begin{aligned}\Delta\mathcal{G}_\alpha(E) = \frac{N_f N_c}{\pi^3} &\int dk\, k^2\, G_{12}(E;k)\,\{1 - 2\,n_F[\omega_Q(k)]\} \\ &\times \int dk'\, k'^2\, G_{12}(E;k')\,\{1 - 2\,n_F[\omega_Q(k')]\} \\ &\times [a_0(k,k')T_{0,a}(E;k,k') + a_1(k,k')T_{1,a}(E;k,k')].\end{aligned} \tag{32}$$

The coefficients a_l result from the traces over the spinor structure. In line with the above approximation of neglecting spin-induced interactions, we use a $1/m_Q$ expansion for these coefficients (which also leads to the degeneracy of pseudoscalar-vector and scalar-axialvector). One has [7]

$$a_0 = 2 \qquad a_1 = 0 \tag{33}$$

for S waves and

$$a_0 = 0 \qquad a_1 = -2\frac{k\,k'}{m_Q^2} \tag{34}$$

for P waves.

To test or quarkonium spectral functions against lQCD correlators, computed with good accuracy in Euclidean spacetime, we need to calculate the Euclidean-time correlator defined as

$$\begin{aligned}G_\alpha(\tau,T) &= \int dE\,\sigma_\alpha(E,T)\,\mathcal{K}(\tau,E,T), \\ \mathcal{K}(\tau,E,T) &= \frac{\cosh[E\,(\tau - \beta/2)]}{\sinh[E\beta/2]}.\end{aligned} \tag{35}$$

The use of a constant width in the two-particle propagator, Eqs. (16), implies a nonvanishing value for $\sigma_\alpha(E \to 0)$. This induces an artificial singularity in the Euclidean correlator since the temperature kernel, $\mathcal{K}$, diverges in the zero-energy limit. This is an artifact of the quasiparticle approximation that can in principle be cured by employing a microscopic calculation of the single-particle self-energies leading to the proper limit, $\sigma_\alpha(E \to 0) \to E$, for the retarded meson spectral function. We defer this study to future work and evade the singularity problem by imposing a cutoff below which we set the imaginary part of the propagator to zero, $E_{\rm cut} = 2(8)$ GeV for charmonia (bottomonia). Note that these cutoff values are far away (by several factors of the quasiparticle width) from bound-state location. Thus, there is very little sensitivity to our correlator results when decreasing $E_{\rm cut}$ by up to a factor of 2.

An additional subtlety in the comparison of model spectral functions to lQCD Euclidean correlators [51–53] is the presence of so-called zero-mode (ZM) contributions. These may be pictured as changing the time direction of a HQ line and thus represent HQ scattering processes, including Landau damping (rather than $Q\bar{Q}$ propagation). It turns out that the pseudoscalar quarkonium channel does not pick up the ZM contribution. To avoid extra uncertainties due to the latter, we therefore restrict our comparisons to Euclidean lQCD correlators to this channel [recall that within our approximations the S-wave pseudoscalar (η_c) and vector (J/ψ) channels are degenerate]. A common way to display the Euclidean correlator at a given temperature uses a normalization to a so-called reconstructed correlator, which uses a baseline spectral function (e.g., the vacuum one) with the Kernel $\mathcal{K}$ at the same temperature as in numerator,

$$R_\alpha(\tau;T) = \frac{\int dE\,\sigma_\alpha(E,T)\,\mathcal{K}(\tau,E,T)}{\int dE\,\sigma_\alpha(E,T_{\rm rec})\,\mathcal{K}(\tau,E,T)}. \tag{36}$$

The idea underlying this ratio is to exhibit the temperature effects on the in-medium spectral function, $\sigma_\alpha(E,T)$ relative to a baseline spectral function, $\sigma_\alpha(E,T_{\rm rec})$, and thus to reduce the effects of systematic uncertainties (e.g., discretization effects in lQCD which distort the high-energy part of the spectral functions). As pointed out in Ref. [7] the spectral function used in the reconstructed correlator can have significant impact on the normalization and shape of $R_\alpha(\tau;T)$. Here, we always use our calculated vacuum spectral function as baseline, i.e., $T_{\rm rec} = 0$.

Let us finally elaborate on the diffusion properties of a single heavy (anti-) quark which we evaluate in terms of the heavy-light quark T matrix. As discussed in the previous paragraph, the zero-energy limit of the quarkonium spectral function in the vector channel can be related to (large-wavelength) HQ transport [51–53]. In principle, this can be used to extract the HQ diffusion constant (at vanishing HQ momentum). However, the 3D reduction underlying the T-matrix approach eliminates the contributions from antiparticles which are needed to exploit this connection, since the zero-mode contribution involves reversing a quark (or antiquark) line in the quarkonium correlator into its antiparticle line. At the same time, this operation identifies the transport contribution as a scattering process of a single heavy quark. Here, we compute this process explicitly (and for arbitray HQ momentum) using the same interaction kernel as in the quarkonium channel by substituting one of the heavy quarks by a light quark (note that the static approximation remains valid for an in- and outgoing on-shell heavy quark). Following Ref. [54], one may

approximate the Boltzmann equation for the HQ distribution function in the QGP by a Fokker-Planck equation and extract the pertinent thermal relaxation rate (inverse relaxation time) as

$$\gamma_c = 1/\tau_Q \equiv \lim_{p\to 0} A(\vec{p}\,) \tag{37}$$

with the friction coefficient

$$A(\vec{p}\,) = \frac{1}{16\,(2\pi)^9\,\omega_Q(p)} \int \frac{d^3q}{\omega_q(q)}\, n_F[\omega_q(q)] \int \frac{d^3q'}{\omega_q(q')} \times \int \frac{d^3p'}{\omega_Q(p')} \frac{(2\pi)^4}{d_c} \sum |M|^2\, \delta^{(4)}(q+p-q'-p') \times \left(1 - \frac{\vec{p}\cdot\vec{p}\,'}{\vec{p}^{\,2}}\right). \tag{38}$$

The invariant amplitude squared, which is summed over color, angular momentum, spin, and light-flavor degrees of freedom (and averaged over the $d_c = 6$ initial spin-color states of a heavy quark), is calculated in terms of S and P waves on-shell T matrices as

$$\sum |M|^2 = \frac{64\pi}{s^2}\left(s - m_q^2 + m_Q^2\right)^2 \left(s - m_Q^2 + m_q^2\right)^2 \times N_f \sum_a d_a (|\tilde{T}_{a,0}(s)|^2 + 3|\tilde{T}_{a,1}(s)\,\cos(\theta_{cm})|^2), \tag{39}$$

where[5]

$$\tilde{T}_{a,i}(s) \equiv m(p_{\text{c.m.}})^{1/2}\, T_{a,i}(E,\, p_{\text{c.m.}},\, p_{\text{c.m.}})\, m(p_{\text{c.m.}})^{1/2} \tag{40}$$

with center-of-mass (c.m.) energy and momentum

$$E = \sqrt{s} = \omega_q(p_{\text{c.m.}}) + \omega_Q(p_{\text{c.m.}})$$
$$p_{\text{c.m.}} = \frac{1}{2E}\sqrt{m_Q^4 + \left(m_q^2 - s\right)^2 - 2m_Q^2\left(m_q^2 + s\right)}\,.$$

The color degeneracy factors are given by

$$d_0 = 1, \quad d_{\bar{3}} = 3, \quad d_6 = 6, \quad d_8 = 8. \tag{41}$$

In Eq. (38), the distribution functions, n_F, include up (u), down (d), and strange (s) quarks in the thermal heat bath with incoming (outgoing) three-momentum, $\vec{q}$ ($\vec{q}\,'$). The in- and outgoing HQ three-momenta are $\vec{p}$ and $\vec{p}\,'$. As an extension to previous work [6,56] we here distinguish explicitly between light- and strange-quark contributions (instead of using light quarks with an effective degeneracy of $N_f = 2.5$). In accordance with HQ spin symmetry (as adopted in the quarkonium sector) we assume degeneracy of S waves (e.g., pseudoscalar D and vector D^* mesons) and of P waves (e.g., scalar D_0 and axialvector D_1 mesons). In our numerical calculations below we also evaluate the contributions from HQ scattering off gluons. In this case, a potential picture is less straightforward. Therefore, as in previous work [6,56], we account for elastic HQ-gluon scattering via the leading order perturbative diagrams (including a Debye screening mass) with a rather large coupling constant of $\alpha_s = 0.4$.

[5]Due to the slightly different definition of the relativistic factors in our T matrix compared to Ref. [6] the connection to the cross section is modified [55].

C. Summary of parameter fixing

Before we turn to the discussion of our numerical results for HQ and quarkonium properties in the QGP, we here summarize the parameters figuring into the calculations, how they are fixed, and what the main corresponding uncertainties are.

1. Interaction potential

The four parameters characterizing the strength [$\alpha_s(T)$, $m_G^2(T)$] and screening [$m_D(T)$, $\tilde{m}_D(T)$] of the color-Coulomb and string potential, respectively, are fit at each temperature to lQCD computations of the color-average $Q\bar{Q}$ free energy. Uncertainties in these parameters are estimated by using two different lQCD computations of this quantity, namely for 2+1 [12,39,40] and three-flavor QCD [13,41]. The uncertainties in the concpetual extraction of a $Q\bar{Q}$ potential are estimated by using either the free or internal energy for both cases, believed to bracket the magnitude of possible interaction strengths.

2. Heavy-quark self-energy

The real part of the single HQ self-energy in medium is identified with (half of) the long-distance limit of the extracted potential, $\text{Re}\ \Sigma_Q(T) = X(r\to\infty, T)/2$, and assumed to be momentum independent. For the imaginary part of the single HQ self-energy, our default is the "narrow-width limit" with $\text{Im}\,\Sigma_{Q,\bar{Q}}(T) = -\Gamma_{Q,\bar{Q}}/2 = -0.01$ GeV, translating into a quarkonium bound-state width of $\Gamma_{Q\bar{Q}} = 0.04$ GeV, for numerical and plotting purposes. To illustrate the uncertainty in the width, we also perform calculations with a (constant) large HQ width of $\Gamma_{Q,\bar{Q}} = 0.1$ GeV, which affects quarkonium correlator ratios and HQ diffusion coefficients by less than 10%. However, the "apparent" quarkonium melting temperatures as estimated from the disappearance of the peak in the spectral function are affected significantly (e.g., reduced by ca. 20% for ground-state charmonium).

3. Quark masses

In addition to the self-energy of the heavy quark its temperature-independent bare mass has to be fixed, cf. Table I. This is done by requiring that, for each potential separately, the charmonium and bottomonium ground-state mass in vacuum result at their empirical value (more precisely, at the average η_c-J/ψ and Υ-η_b mass since we neglect hyperfine splitting in this work). In addition, for the calculation of the heavy-light T matrix, the light quark mass has to be fixed. In the vacuum, we merely check whether the use of typical constituent quark masses for u, d ($m_{u,d} = 0.4$ GeV) and s quarks ($m_s = 0.55$ GeV), believed to arise from chiral symmetry breaking, lead to reasonable values for ground-state D, D_s and B, B_s masses. In the QGP, we adopt thermal parton masses proportional to gT such that the corresponding quasiparticle equation-of-state of the QGP is in line with the ca. 10% reduction relative to the massless gas as found in lQCD [57]. The same g is used to compute the gluon scattering contribution to HQ diffusion in leading-order pQCD. As

TABLE I. Dependence of the bare HQ masses on the 3D reduction scheme and underlying lattice potential when adjusting the ground-state quarkonium mass to the average experimental value. Also quoted are the effective light- and strange-quark masses which have been adjusted to the average heavy-light meson ground-state mass.

		BbS scheme	Th scheme
Potential 1	m_c^0	1.355 GeV	1.264 GeV
	m_b^0	4.712 GeV	4.662 GeV
Potential 2	m_c^0	1.402 GeV	1.293 GeV
	m_b^0	4.768 GeV	4.700 GeV
$m_q = 0.4$ GeV, $m_s = 0.55$ GeV			

noted in Ref. [6] the values of the light-parton masses and widths have very little impact on the HQ diffusion coefficient, while the gluon contribution as calculated here is subleading compared to the heavy-light T matrix. Thus our results for the HQ diffusion coefficient are rather insensitive to the QGP quasiparticle properties and the value used for g. They are much more sensitive to whether the internal or free energy is being used as interaction kernel.

4. Numerical parameters

Finally, there are three parameters of an essentially numerical nature: the energy cutoff, $E_{\rm cut}$, in the evaluation for the Euclidean correlatros, Eq. (36), and the parameters Δ and Λ in the off-shell extension of the running coupling constant, Eq. (26). We have verified that factor-2 variations in these parameters have negligible impact on our results.

We believe that, with the model input and pertinent parameters fixed as sketched above, and with constraints from lQCD, the pQCD limit and vacuum spectroscopy, the in-medium T-matrix approach allows to establish useful connections between quarkonium properties and HQ transport in the QGP.

IV. SPECTRAL FUNCTIONS, CORRELATORS, AND RELAXATION TIMES

In this section we first fix the bare heavy-quark masses—as well as light- and strange-quark masses—and check the resulting spectral functions against vacuum spectra of hidden and open heavy-flavor mesons (Sec. IV A). We then discuss our numerical results for quarkonium spectral functions and pertinent Euclidean correlators with emphasis on the uncertainties originating from the choice of potential and reduction scheme (Sec. IV B). Finally, we apply our formalism to evaluate HQ thermalization times and diffusion coefficients (Sec. IV C).

A. Vacuum spectroscopy and quark masses

Let us first focus on the vacuum spectra of charmonia and bottomonia to determine the bare masses of charm (c) and bottom (b), $m_{c,b}^0$, which figure into the expression for the effective mass, Eq. (12). We do this by requiring the S-wave charmonium (bottomonium) ground state to occur at the average mass of η_c and J/ψ at $\sim$3.04 GeV, and at the $\Upsilon(1S)$ mass of $\sim$9.46 GeV (we neglect hyperfine splittings); see Fig. 8. Since the entropy term in the HQ free energy vanishes in the vacuum there is no difference between the free and internal energy. The resulting bare-quark masses are compiled in Table I for the two different potentials and reduction schemes. They generally fall into the range expected from the bare masses quoted by the particle data group [58] and are also consistent with previous T-matrix calculations [7]. The spread (in particular the relative one) is somewhat larger in the charm sector (ca. 140 MeV) than in the bottom sector (ca. 100 MeV), in line with the expectation that the 3D reduction becomes more reliable with increasing mass. The mass gap between the ground and first excited charmonium state varies rather little between the two potentials within a given reduction scheme, $\delta m_\psi = 0.65$–0.68 GeV (BbS) and 0.54–0.56 GeV (Th). Compared to the experimental value of $m_{\psi'} - m_{J/\psi} = 0.59$ GeV, the Thompson scheme seems to be doing slightly better (the bare masses in the BbS scheme tend to be slightly high). The situation is opposite for the pseudoscalar mass splitting between η_c and $\eta_c(2S)$, where the BbS scheme does slightly better (however, the effects of the hyperfine splitting are expected to be larger in the pseudoscalar than in the vector case). The Th scheme appears to perform somewhat better again for the χ_c states, for which the BbS scheme overpredicts the spin-averaged mass by up to 0.1 GeV. From these observations we deduce an overall uncertainty of our T-matrix approach of 50–100 MeV in the charmonium sector, comparable to corrections one expects from hyperfine splittings.

In the bottomonium sector (lower panels in Fig. 8), the mass gaps between the ground state Υ and the first exited state, as well as between the first and second exited states, are reproduced within 30 MeV (BbS) and 70 MeV (Th). The differences in the potentials have again only minor impact. A similar trend is found for the spin-averaged masses of the χ_b states: using the BbS scheme our results tend to be higher in mass (especially for potential 2) compared to the experimental values for $m_{\chi_{b0}}$ and $m_{\chi_{b2}}$, while for the Th scheme we typically obtain results 30 MeV below experiment. In addition, for both reduction schemes and potentials, we obtain a $\chi_b(3S)$ state right at the continuum threshold. Since there is no experimental evidence for this state, this could again be indicative for some overbinding. Recall, however, that we do not account for residual B-$\bar{B}$ interactions in our single-channel treatment, which could have a significant impact on the spectral function especially close to threshold. As to be expected, the difference in the Coulomb term of the two vacuum potentials (different α_s but equal string tension) induces larger deviations for the more deeply bound bottomonia, while the sensitivity to the reduction scheme (static approximation) is reduced. Overall, the accuracy of the predictions of our T-matrix approach is at the 10% level of the $1S$-$2S$ mass splittings. This is of the same order (or even below) the observed hyperfine splittings. This seems reasonable given that we have neglected both spin-spin and spin-orbit interactions at the quark level, as well as residual mesonic interactions in $D\bar{D}$ and $B\bar{B}$ channels.

Finally, the values of light- and strange-quark mass have to be fixed. Since the physics of their effective vacuum masses differs from than in the HQ sector (spontaneous chiral

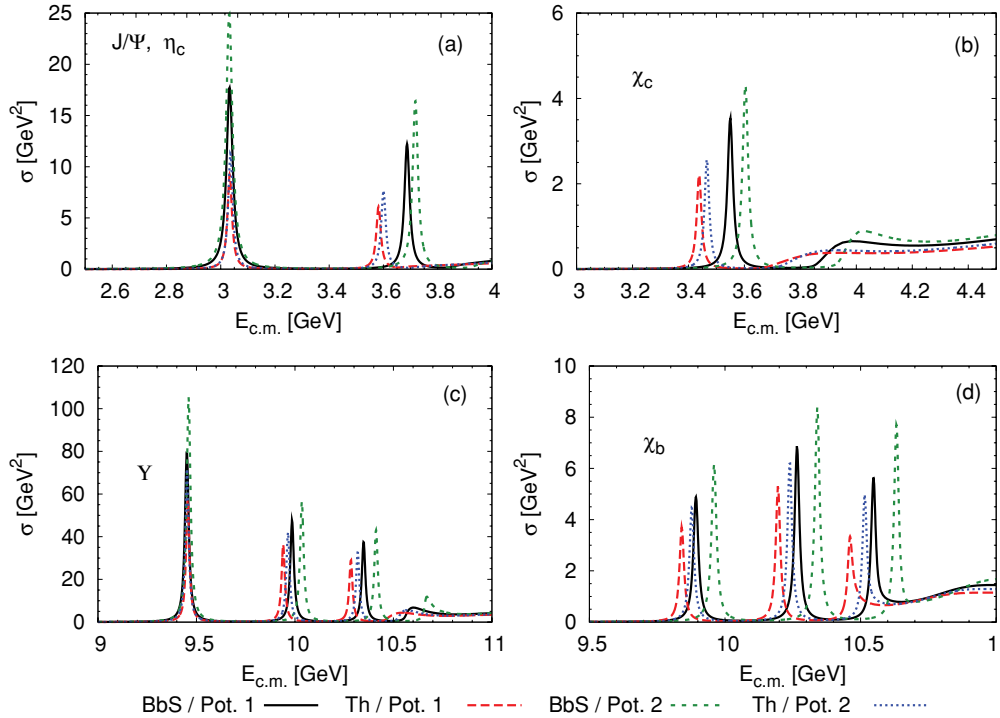

FIG. 8. (Color online) Quarkonium spectroscopy in vacuum for S- and P-wave charmonia (upper panels) and S- and P-wave bottomonia (lower panels).

symmetry breaking vs. string breaking), we directly adjust the constituent masses. With $m_q = 0.4$ GeV we obtain a S-wave D-meson mass of 2.01(2.02) GeV in the Th (BbS) scheme which coincides with the experimental value for the D^* meson (but is larger than the average D-D^* mass by ca. 60–70 MeV), see Fig. 9. It turns out that both smaller and larger m_q lead to a larger D-meson mass: in the former case the increase in kinetic energy dominates, while in the latter case the increase in mass is more important. The result for the D-meson mass is roughly consistent with the string-breaking scale in the HQ potential, in the sense that the $D\bar{D}$ threshold (=twice the D-meson mass) approximately coincides with twice the separation energy of the $Q\bar{Q}$ pair plus their bare masses,

$$2m_D \simeq V(r_{\rm SB}) + 2m_c^0 = 2m_c. \tag{42}$$

In this interpretation, the binding energy of the heavy-light system should coincide with the constituent light-quark mass. This is roughly satisfied in the charm sector (m_D is ∼3–10% larger than m_c) while the agreement improves in the bottom sector. Interesting effects are found in the nonsinglet color channels (which will figure into our calculations of HQ transport in Sec. IV C below); cf. Fig. 9. In the color-antitriplet diquark channel, where the Coulomb term brings in half of the attraction as in the mesonic (color-singlet) channel, a bound state is observed at about $m_{Qq} \simeq 2.1 \pm 0.05$ GeV, corresponding to a binding energy of ca. 0.15 GeV. To construct a charmed baryon, one may imagine to add another light quark with an estimated binding of ∼0.25 GeV, in analogy to the D meson. The resulting baryon mass would amount to ∼2.25 GeV, not far from the empirical Λ_c mass of 2.29 GeV. The color-Coulomb is repulsive in the sextet and octet channels, implying that the states at around ∼2.2 GeV are entirely due to the confining force. It is tempting to speculate that the binding of an octet and antioctet (or sextet and antisextet), with a binding energy comparable to the ground-state charmonium, ∼0.6 GeV, could be a relevant configuration underlying the recently discovered X, Y, and Z states in the 3.8–4.5 GeV mass region. The small widths of these states would be naturally explained due to their predominantly color nonsinglet building blocks; see also Refs. [59–61]. If this picture is correct, one predicts further regimes of rich spectroscopy for narrow "exotic" four-quark states around masses of 6 GeV ($2c2\bar{c}$), 10 GeV ($b\bar{b}q\bar{q}$, $2b2\bar{q}$, $2\bar{b}2q$), and 20 GeV ($2b2\bar{b}$).

The empirical heavy-strange mesons, D_s and D_s^*, are ca. 100 MeV heavier than the nonstrange states (D and D^*). We can reproduce this splitting by choosing a constituent strange-quark mass of $m_s = 0.55$ GeV, consistent with typical values in constituent quark models. Other properties of the cs states are quite similar to our findings for the cq states and will not be reiterated here. This also applies to the open-bottom bq and bs states.

B. Quarkonium spectral and correlation functions in the quark-gluon plasma

With all parameters fixed and in-medium potentials determined we now proceed to compute the spectral functions of heavy quarkonia in the QGP. These can be tested by comparing the pertinent Euclidean correlator ratios, Eq. (36), to computations of this quantity on the lattice. Recent results

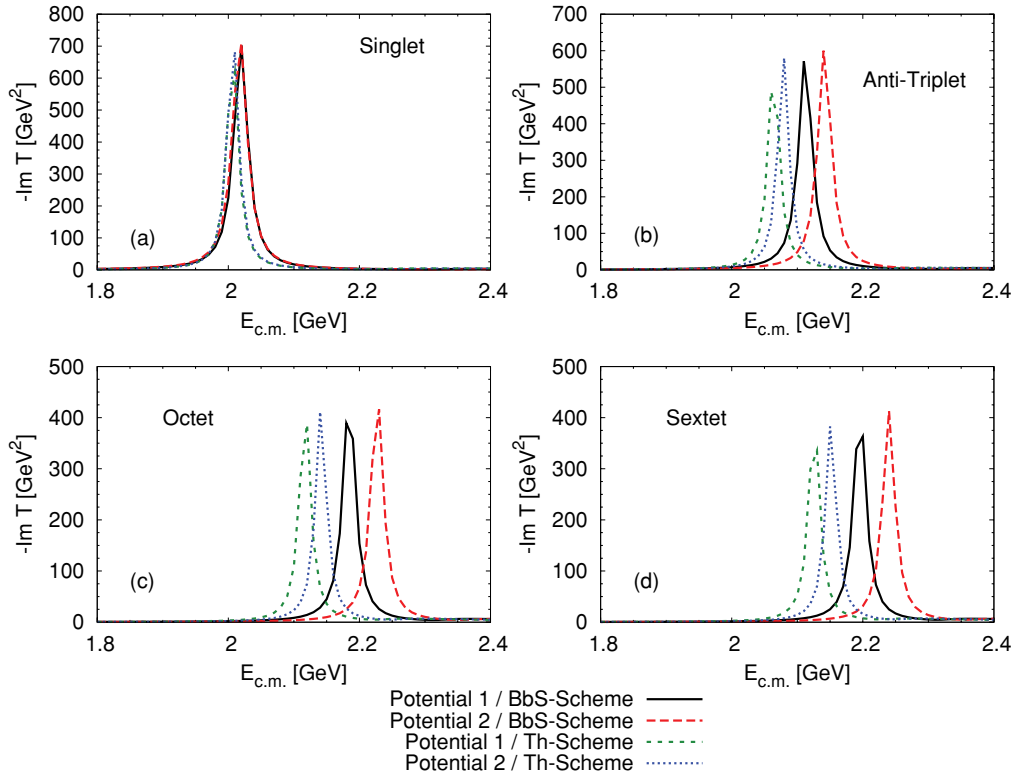

FIG. 9. (Color online) Imaginary part of the charm-light T-matrix in the vacuum using $m_q = 0.4$ GeV. We show the color singlet $Q\bar{q}$ (upper left plot), antitriplet Qq (upper right plot), octet $Q\bar{q}$ (lower left plot), and sextet Qq (lower right plot) channels.

by Jakovác *et al.* [62] in quenched QCD and by Aarts *et al.* [63] for $N_f = 2$ show small variations of about 10% of the correlator ratios for charmonia up to temperatures of about 2 T_c, and even less for bottomonia. Such a behavior could be semiquantitatively reproduced in several potential model approaches [7,16,17,64]. However, no systematic assessment of relativistic corrections has been performed in these works.

We limit our in-medium investigations to the temperature regime $T \geqslant 1.2\,T_c$; closer to T_c, the infnite-distance limit of the internal energy, $U_\infty(T)$, exhibits a rapid increase which is presumably associated with the onset of phase-transition dynamics. We do not expect pertinent effects to be properly accounted for in our current single-channel ($Q\bar{Q}$) implementation of the T matrix (e.g., close to a second-order phase transition, long-range many-body correlations become important, as well as new degrees of freedom such as $D\bar{D}$ channels, which are not included here). We also recall that at this point we do not include hyperfine (spin-spin) interactions, energy-momentum dependencies of the HQ self-energies, nor additional coupled channels (e.g., singlet-to-octet transitions involving an extra gluon from the heat bath [9]). Therefore, we believe that quantitative comparisons beyond the 10% acccuracy level referred to above are not yet warranted but will be conducted in future work once (some of) the neglected effects are accounted for.

In the following, we divide the presentation into the charmonium (Sec. IV B1) and bottomonium (Sec. IV B2) sectors, followed by a combined evaluation (Sec. IV B3).

1. Charmonium

We begin our in-medium analysis for the S- and P-wave channels in the charmonium sector using a small "numerical width" of 20 MeV for the c and $\bar{c}$ quarks (recall the degeneracy of pseudoscalar-vector as well as of scalar-axialvector states). Contrary to the vacuum, we now distinguish two scenarios depending on whether the free (F) or internal (U) energy is identified as the static finite-temperature potential. The results are compiled in Figs. 10 and 11 for U and in Figs. 12 and 13 for F as potential.

Let us first focus on the former case, $V(r;T) = U(r;T) - U_\infty(T)$. At the level of the in-medium spectral functions both lQCD inputs and reduction schemes share a number of generic trends, all of which were already present in the T-matrix calculations of Ref. [7]. The S-wave ground state (η_c, J/ψ) survives as a bound state up to temperatures of about 2–2.5 T_c around which it merges into the $c\bar{c}$ continuum. But even at temperatures as low as 1.2 T_c the medium effects in the potential induce a reduction of the binding energy, $E_B = 2m_c - m_\psi$ by about a factor of $\sim$2, to $E_B \simeq 0.3$–0.4 GeV compared to 0.6–0.8 GeV in the vacuum (for Th and BbS, respectively). The effective quark mass at this temperature is approximately the same as in vacuum, causing a net increase in the mass of the S-wave ground state to $m_\psi(1.2T_c) \simeq$ 3.3–3.4 GeV. For higher temperatures, the binding further decreases but this effect is overcompensated by a reduction in the effective charm-quark mass [i.e., in $U_\infty(T)/2$], so the mass of the state actually decreases. Along with the decrease in binding goes a reduction in the strength of the state

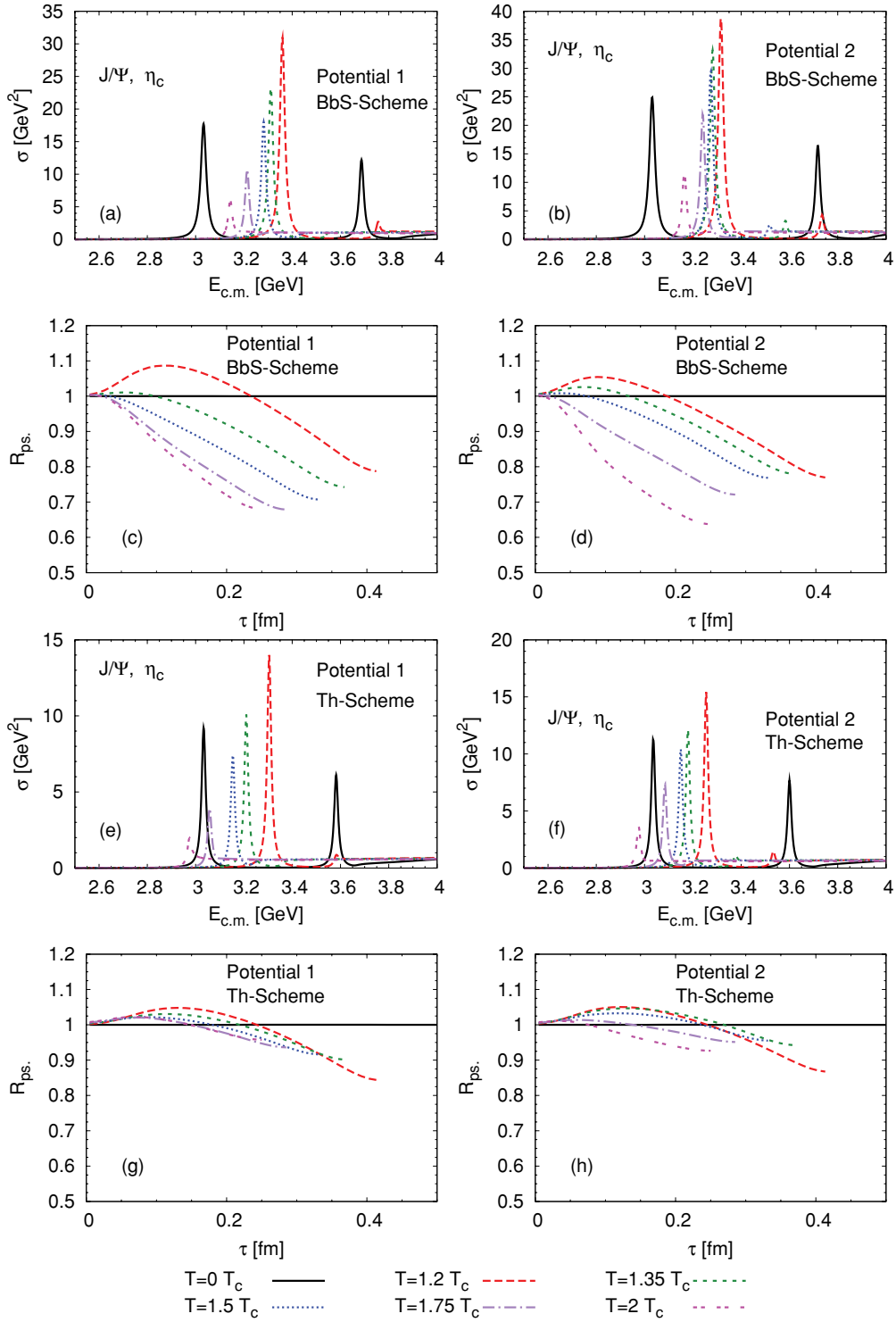

FIG. 10. (Color online) Charmonium spectral functions and Euclidean correlators in the pseudoscalar (S-wave) channel at various temperatures using the internal energy (U) as potential. Results for two reduction schemes and two different potentials are compared.

(=peak height of the spectral function at fixed width). The rather subtle differences in the spectral functions become more apparent in the Euclidean correlator ratios, especially between the two reduction schemes (within a given reduction scheme, the two different potentials lead to small variations also for the correlator ratios). For the BbS scheme, the ratios deviate by up to 30–40% from one for temperatures of 1.2–2 T_c. This is too large compared to the 10–15% reduction that has been found in lQCD computations [62,63,65]. However, employing the Thompson scheme, the correlator ratios are within 15% from 1, which is better in line with lQCD. The technical reason for the difference in the correlator ratios between BbS and

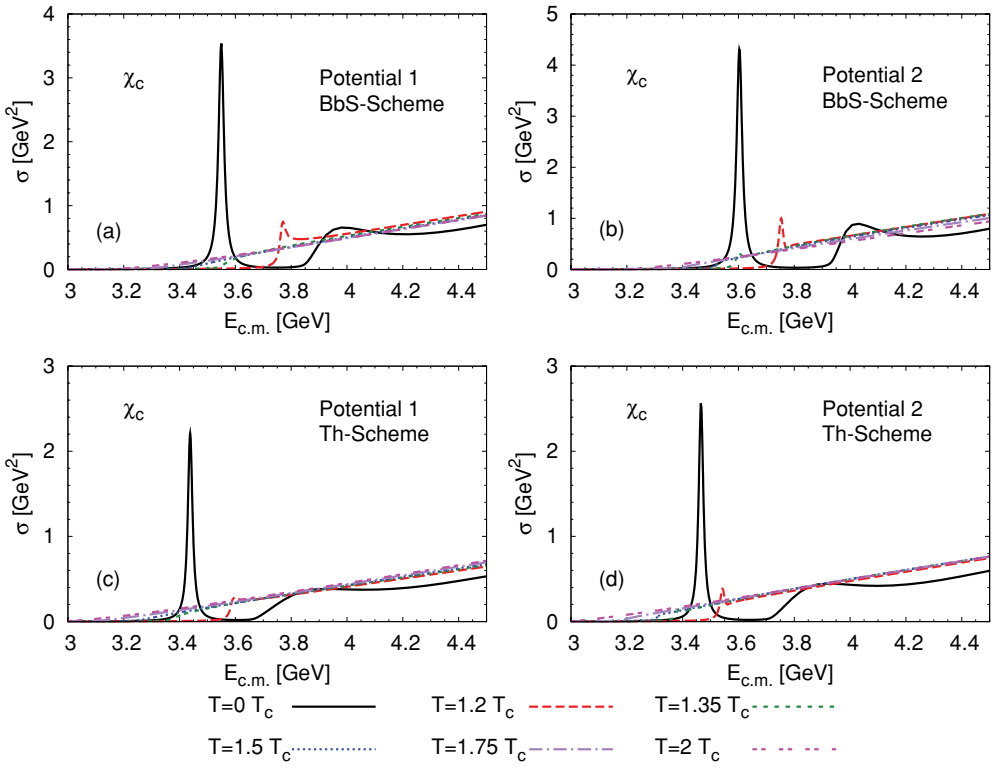

FIG. 11. (Color online) Charmonium spectral functions in the scalar (P-wave) channel at various temperatures using the internal energy (U) as potential. Results for two reduction schemes and two different potentials are compared.

Thompson scheme can be traced back to the larger binding that the BbS scheme generates already in the vacuum. This requires relatively large bare charm-quark masses (recall Table I) which in the medium ultimately lead to too large a ground-state mass (or continuum threshold) when the latter approaches its dissolution [note that in the BbS scheme the J/ψ (or η_c) mass at 2 T_c is still significantly above its vacuum mass, while in the Th scheme it has dropped below the vacuum value]. For the ground-state P-wave state (χ_c) we also find that, right above T_c, it is heavier than in vacuum due to the decrease in binding. However, due to its relatively the small binding energy (in vacuum $E_B \simeq 0.22$–0.25 GeV and 0.3–0.35 GeV in the Th and BbS scheme, respectively) it dissolves just above $\sim$1.2 T_c where it merges into the $c\bar{c}$ continuum.

Next we discuss the in-medium charmonium results when using F as potential, $V(r;T) = F(r;T) - F_\infty(T)$, summarized in Figs. 12 and 13. Compared to the use of U, the in-medium binding is appreciably reduced (recall Fig. 5). For example, the binding energy of the S-wave ground state at 1.2 T_c is reduced by about one order of magnitude, and the state dissolves shortly thereafter, at $\sim$1.3 T_c (Fig. 12). The P-wave states have disappeared already just above T_c. At the same time the value of the potential at infinity provides a smaller self-energy correction (see Fig. 3), leading to a smaller effective quark mass and, consequently, a lowered continuum threshold compared to using U. This, in particular, entails no or only a small rise in the in-medium mass of the J/ψ above T_c. For the BbS scheme the drop in effective mass and the reduction in binding nearly compensate each other, leading to a stable J/ψ mass until dissolution. For the Th scheme the smaller bare-quark mass even leads to a net decrease of the in-medium J/ψ mass. The Euclidean correlator ratios are again very similar for the different potentials but exhibit a significantly different τ dependence for the two reduction schemes. For the BbS scheme the deviation relative to the vacuum correlator is up to $\sim$50% while for the Th scheme it is no more than 10%. However, for both schemes the temperature evolution is remarkably stable, with variations of no more than 15% even in the BbS scheme. Thus the rather large overall deviation originates from the reconstructed (vacuum) correlator, where the problem can be traced back to the large bare-quark mass which is required in this scheme due to the large vacuum binding energy.

To further map out uncertainties we consider the influence of a quark width on the correlator ratios. In Refs. [6,8] it has been found that the charm-quark width above T_c may be as large as 0.2 GeV. We injected into Eqs. (16) a value of $\Gamma_Q = 0.1$ GeV for the HQ width and plot the results, using U as potential, in Fig. 14. As an immediate consequence, the J/Ψ width turns out to be about twice the single-quark quark width, as to be expected. The "dissociation" temperature (loosely defined as the temperature where the peak height is reduced to less than twice the height of the continuum) decreases significantly compared to the narrow-width approximation, to about 1.7 T_c: the broadening of the resonance structure simply accelerates the merging with the continuum part. The peak positions (masses) of the narrow-width calculation are basically preserved. The correlator ratios are

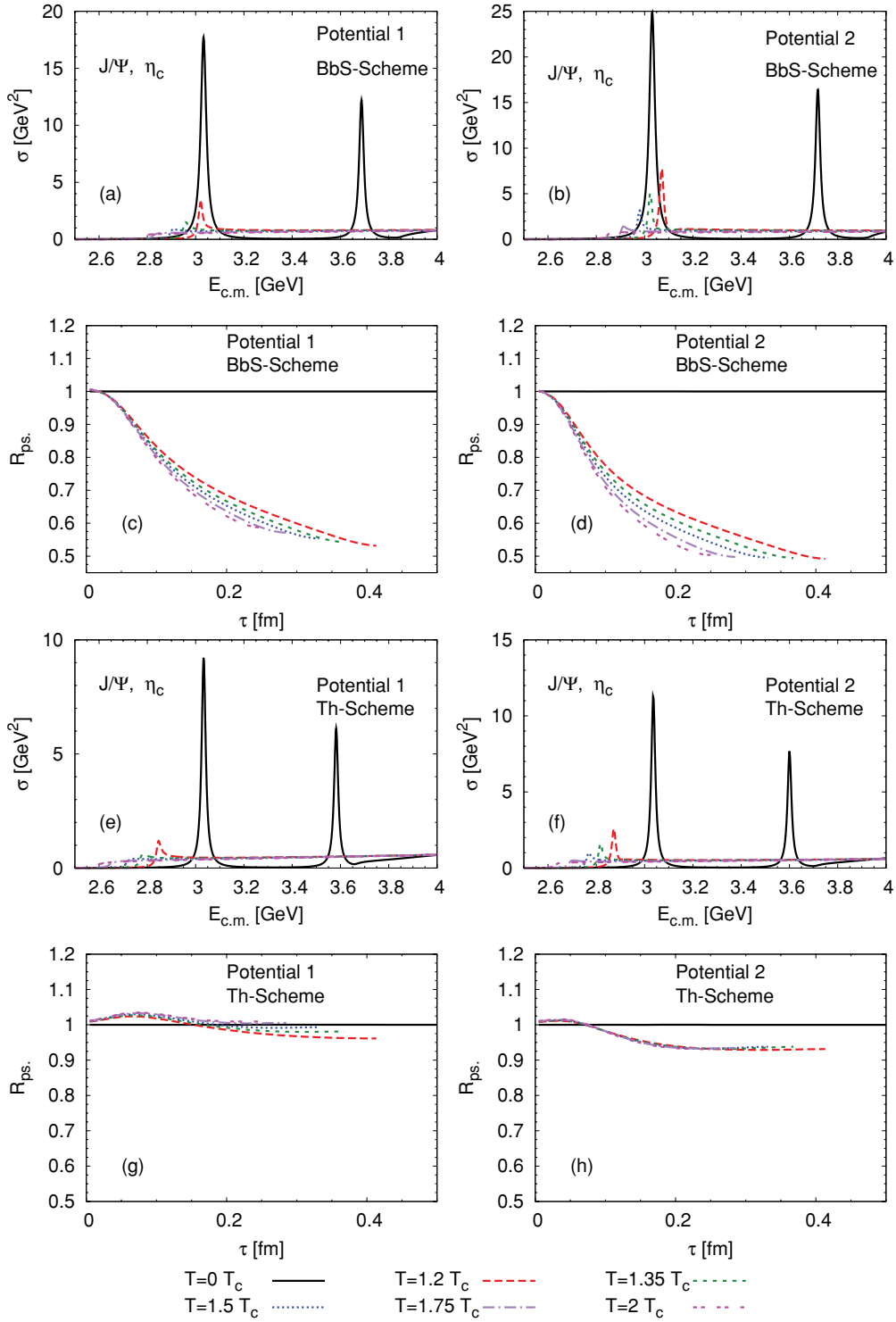

FIG. 12. (Color online) Same as in Fig. 10 but using the free energy (F) as potential.

increased compared to the calculation with small quark widths. The magnitude of the effect is relatively small for the Th scheme where the spread was already small before. For the BbS scheme the increase is more significant: the up to 40% spread in the narrow-width calculation is reduced to within 30%. Similar systematics are also found when using F as potential.

2. Bottomonium

In analogy to the charmonium calculations we supply a small "numerical width" of 20 MeV for the b and $\bar{b}$ quarks. The in-medium bottomonium spectral functions and correlator ratios are compiled in Figs. 15 and 16 for U and in Figs. 17 and 18 for F as potential.

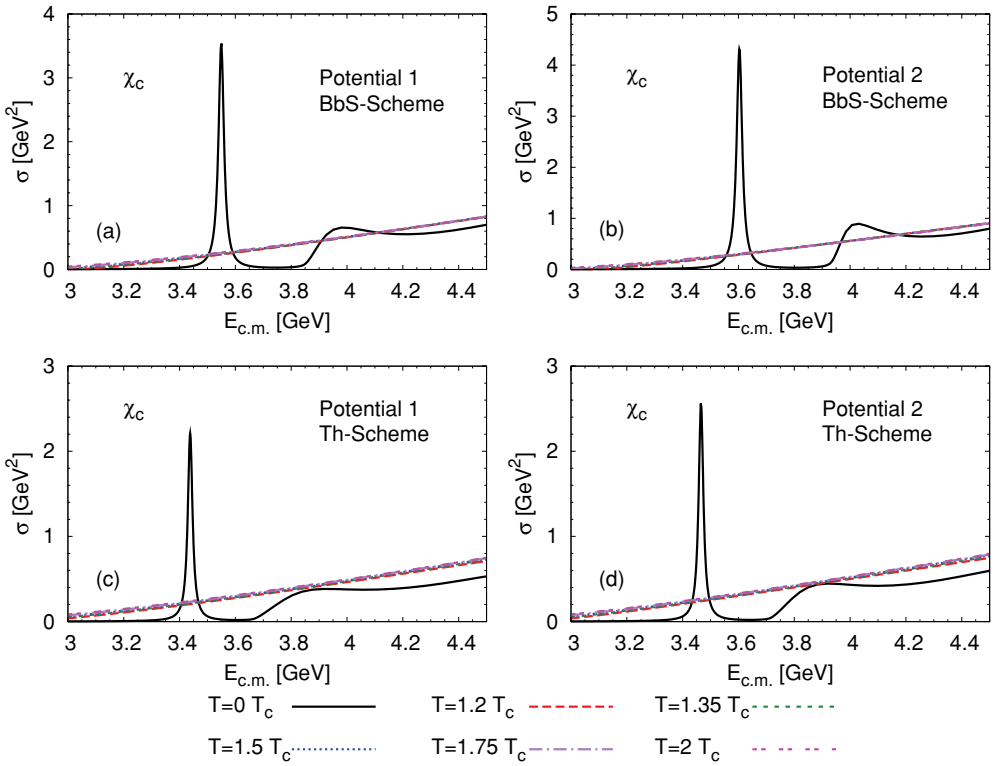

FIG. 13. (Color online) Same as in Fig. 11 but using the free energy (F) as potential.

For the U potential, similar to charmonium, the reduction in binding combined with a large effective quark mass (similar as in vacuum) leads to an increase in the mass of all bottomonium states right above T_c. Within the BbS scheme the mass of the lowest Υ bound state varies by less than 100 MeV over the considered temperature range of 1.2–2 T_c: the lowering of the $b\bar{b}$ threshold and the loss in binding nearly compensate. But even at 2 T_c a well-defined $\Upsilon(1S)$ bound state persists. The $\Upsilon(2S)$ survives up to a temperature of about 1.7 T_c and shows a much larger variation in mass (about 0.5 GeV) while the $\Upsilon(3S)$ basically dissolves at T_c. In the Th scheme we observe a similar pattern. For the Euclidean correlator ratios the calculations within the BbS scheme deviate from one by 20–25%, more than seen on the lattice. However, the relative temperature variations are smaller, ca. 10–15%. In the Th scheme the temperature variations are further reduced to less than 10%, and also the deviations from one are smaller, which is better in line with the essentially constant lQCD correlator ratios close to 1. Further stabilization of our results is conceivable with more realistic in-medium widths and/or improvements in the connection between vacuum and in-medium potentials. For the P-wave χ_b states the ground state melts at about 1.7 T_c while the first excited state dissolves at about 1.2 T_c.

When using F as potential the reduction in binding is again more pronounced, with a dissolution of all excited S-wave Υ's and all χ_b states right at T_c. Only the Υ ground state survives until somewhat above 2 T_c. Compared to the calculation with U as potential the strength of the state at 2 T_c is reduced by a factor of $\sim$3, indicating the lower binding, while its mass is about 200 MeV smaller (the loss in HQ mass overcompensates the loss in binding energy). Also here the temperature dependence of the ground-state mass is rather stable. As before, the Euclidean-correlator ratios are rather sensitive to the interplay of HQ mass, quarkonium binding, and the "pole strength" of the states. The BbS scheme again shows appreciable deviations from one for both potentials, up to 40%, while for the Th scheme these are 10–15%. However, the spread in the temperature dependence is less than 10% for both reduction schemes and lattice inputs. We have verified that the inclusion of larger HQ widths has effects similar as in the charmonium case, increasing the correlator ratios by up to 0.1 units at large τ.

3. Discussion of quarkonium results

Let us try to summarize and evaluate the findings in the quarkonium sector. Within the Th scheme, all S-wave correlator ratios (for both lQCD inputs, for U and F, as well as for charmonium and bottomonium) are within ca. 15% of 1, for all temperatures between 1.2 and 2 T_c. For a given calculation (scenario) the *relative* deviations within this temperature range are, in most cases, even smaller, suggesting that the reconstructed correlators play a non-negligible role in the absolute uncertainty (e.g., "residual" hadronic interactions between D and $\bar{D}$ states in the continuum are not accounted for in a single-channel T matrix as employed here). Within the BbS scheme, we generally find larger deviations of the correlator ratios from 1 (by up to $\sim$50%); within a given scenario, the temperature variations are significantly smaller, up to 30% (or even less especially for the free energy). While this may overestimate the uncertainty associated with the 4D$\rightarrow$3D

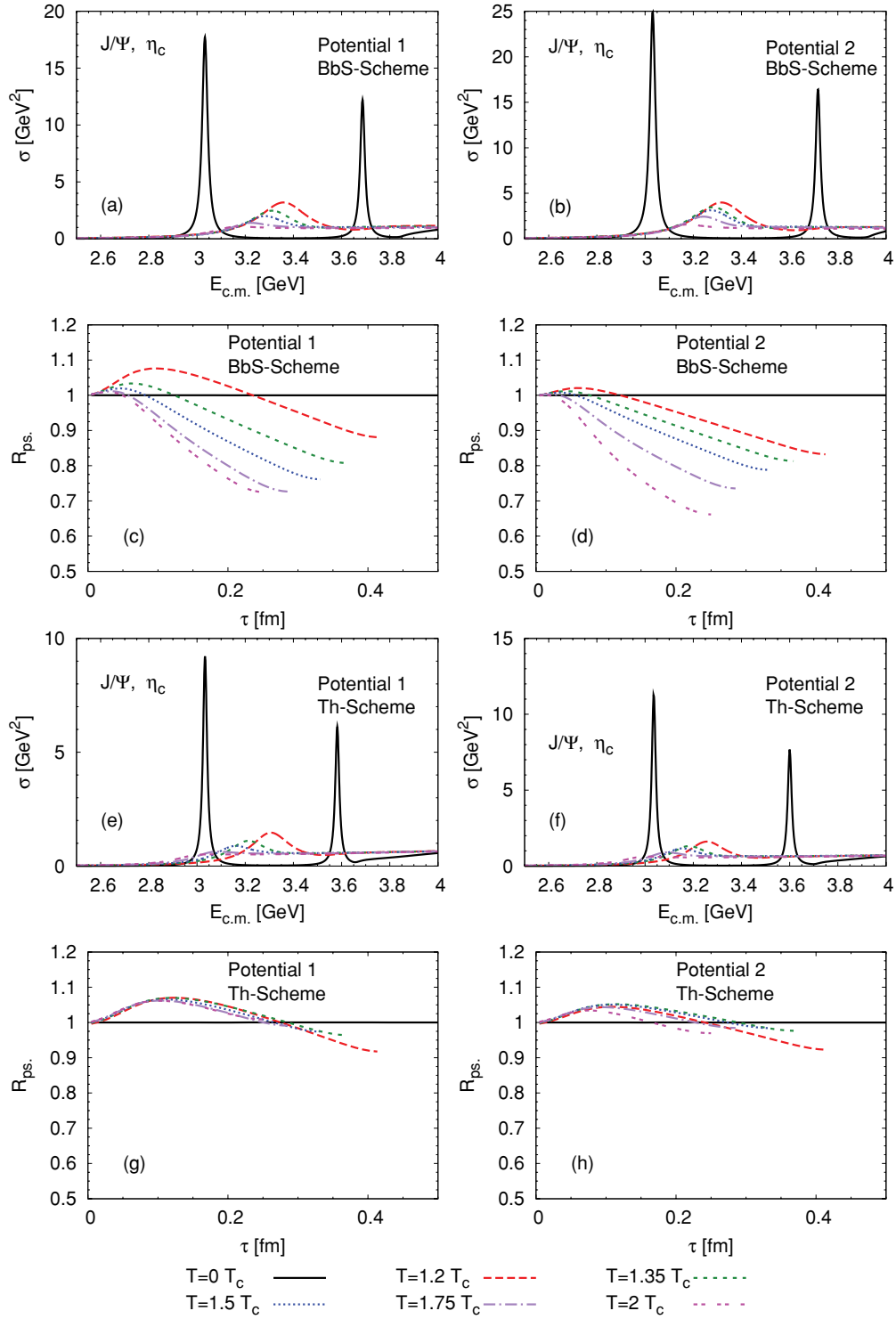

FIG. 14. (Color online) Same as in Fig. 10 but employing a single-quark width of 100 MeV.

reduction scheme (recall that the BbS scheme has a tendency for overbinding, even in vacuum, see also the discussion in Appendix A), it stipulates that the static approximation (especially for charmonia) requires further scrutiny if one aims at an absolute accuracy at the 10% level (applications based on the (nonrelativistic) Schrödinger equation are expected to be beset with larger uncertainty). We have confirmed indications found in Ref. [7] that effects of a finite spectral width are not negligible either, increasing correlator ratios at the 5–10% level. Our schematic implementation of the in-medium widths has only scratched the surface of a full many-body calculation utilizing microscopic single-quark spectral functions

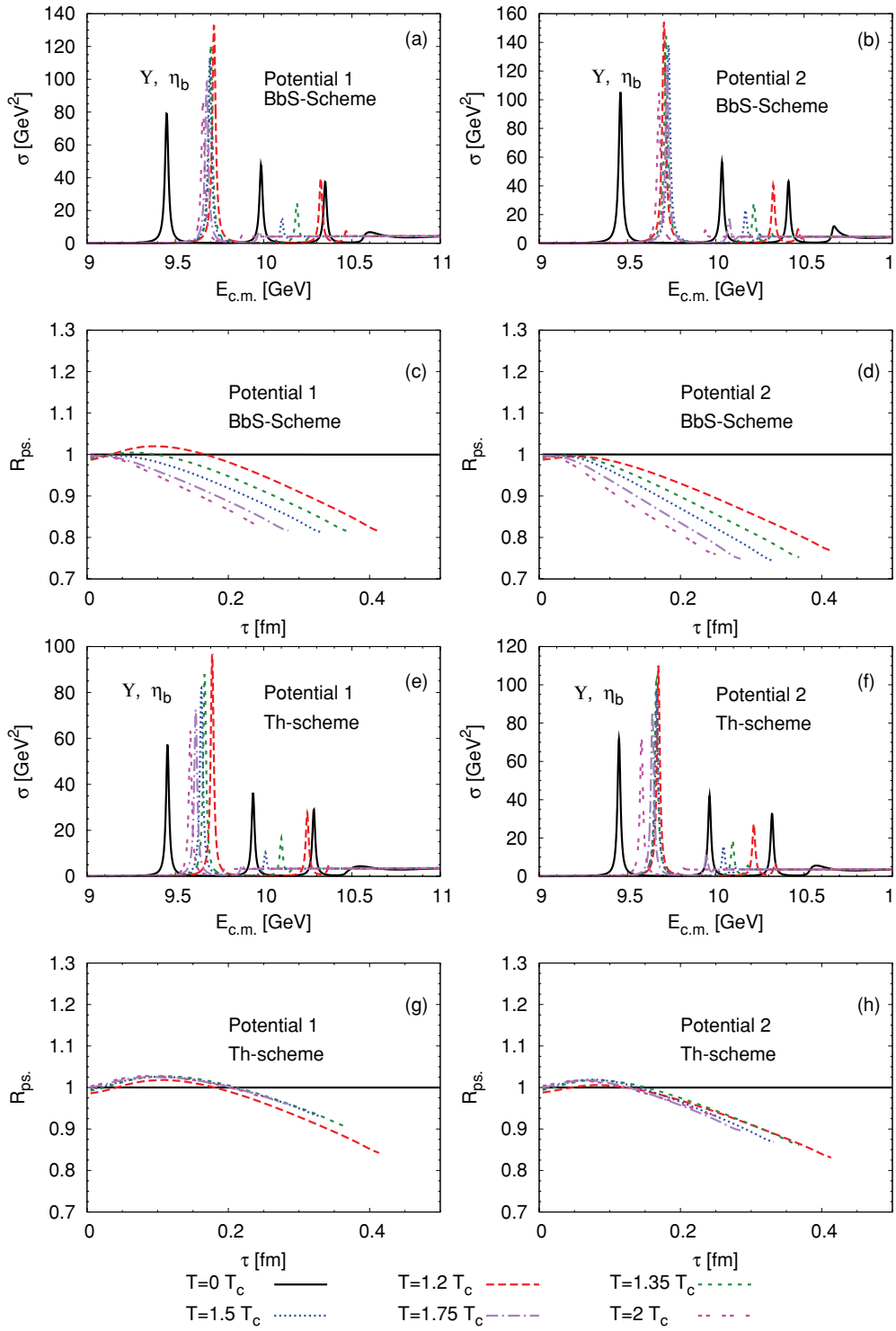

FIG. 15. (Color online) Bottomonium spectral functions and Euclidean-correlator ratios, using U as potential, for the pseudoscalar channel at various temperatures. We compare the BbS and Th schemes as well as the two different potentials.

in the T-matrix equation (see, e.g., Ref. [66] for a recent perturbative calculation of the HQ spectral function in the QGP).

Our analysis corroborates indications from earlier studies [7,16,17,64] that there is currently no decisive discrimination power between the different scenarios realized by the use of U ("strong binding") and F ("weak binding"). When employing U the mechanism underlying a constant (or temperature-stable) correlator ratio is rather involved, being a combination of four components: On the one hand, the binding energies close to (but above) T_c are rather large (several 100 MeV), together with a large pole strength (due to the steepness

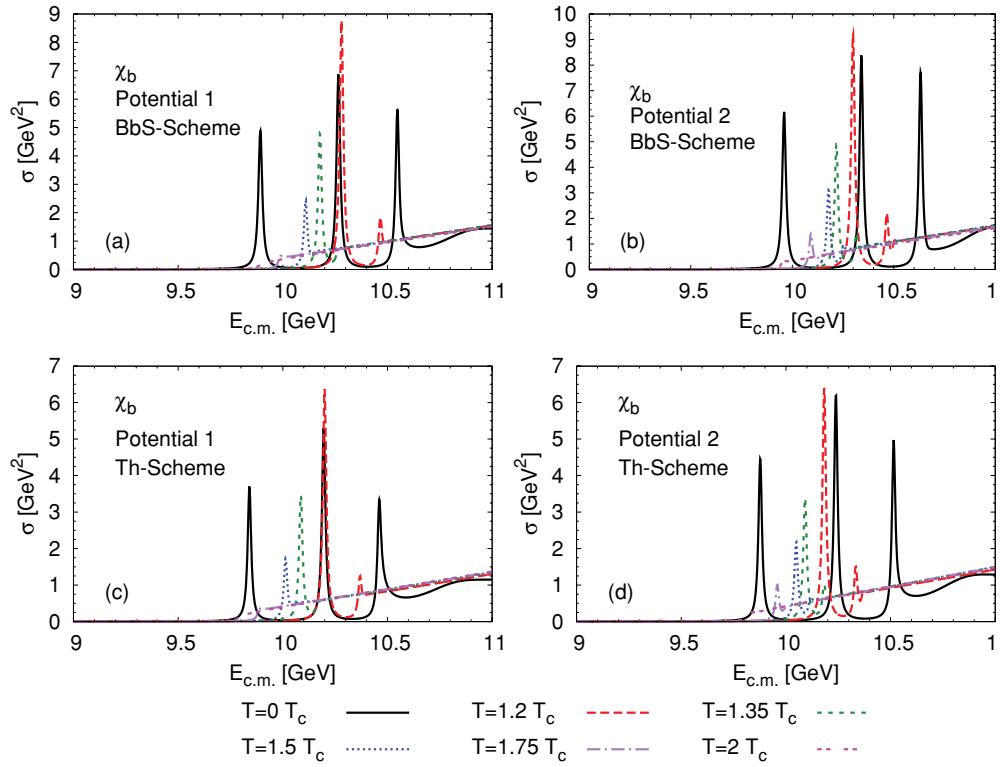

FIG. 16. (Color online) Bottomonium spectral functions using U as potential for the scalar channel at various temperatures using the BbS (upper panels) and Th reduction schemes (lower panels).

of the U potential at intermediate distances). On the other hand, the effective HQ mass, governed by $U_\infty(T)$, and thus the $Q\bar{Q}$ threshold energy, are also large (basically as in vacuum). With increasing temperature, the binding and the pole strength drop, as do the HQ mass and continuum threshold, thus balancing the (low-energy) strength in the spectral function. On the contrary, when employing F, the binding already vanishes just above T_c, and the balance in the spectral function on increasing T is between a further loss of strength in the threshold state (cusp) and a reduction in the HQ threshold. In particular, with the F potential one does not encounter a regime above T_c with a large variation in binding energy. However, going further down in temperature, such a regime must inevitably occur when approaching the vacuum limit, and similar "complications," as in the U-potential calculations above T_c, are to be expected. Thus, a sensitive test of whether the F potential can be consistent with lQCD correlators is in the temperature regime where the largest variation in binding occurs (which is apparently at or below T_c).

C. Heavy-quark diffusion in the quark-gluon plasma

Following the analysis of in-medium quarkonia we now turn to evaluating heavy-flavor transport in the QGP. In the vacuum we have found that the low-lying D-meson spectrum is reasonably well reproduced, but also that shallow bound states might occur in colored heavy-light two-body channels (recall Fig. 9). The calculation of the heavy-light T matrix in the QGP requires an additional input in terms of the in-medium light quark masses [recall that the in-medium HQ self-energy is determined by the infinite-distance of the free/internal energy according to Eq. (12)]. Due to chiral symmetry restoration, the vacuum constituent-quark mass is expected to approach zero; however, the light quarks and gluons most likely acquire (chirally symmetric) thermal masses. We approximate these by adopting the functional form expected from perturbative QCD [67],

$$m_{\rm th}(T) = \sqrt{\frac{1}{3}}\, g\, T, \quad m_q(T) = \sqrt{m_{q,0}^2 + m_{\rm th}^2(T)} \\ m_{u,0} = m_{d,0} = 0, \quad m_{s,0} = 0.11\text{GeV}. \tag{43}$$

When implemented into a quasiparticle (QP) description of the QGP this form allows to recover an energy density, $\epsilon_{\rm QP}$, which is roughly 10–20% below the perturbative value, independent of temperature [68,69]. We fix the strong coupling in Eq. (43) at $g = 2.3$, resulting in $\epsilon_{\rm QP}/\epsilon_{\rm SB} \simeq 0.83$, consistent with recent lQCD calculations [57] for $T \geqslant 1.4T_c$. This value for g is also compatible with our perturbative calculations for scattering off thermal partons ($\alpha_s \simeq 0.4$).

In Fig. 19 we compile in-medium charm-light T matrices using U for potential-1 within the Th scheme, with an in-medium single-quark width of 100 MeV (uncertainties due to reduction scheme and potential are exhibited in the context of the thermal relaxation rates below). In the medium the color-sextet and -octet correlations fade rapidly due to screening of the attractive string part of potential (recall Fig. 5). The meson (color-singlet) and diquark (color antitriplet) channels feature

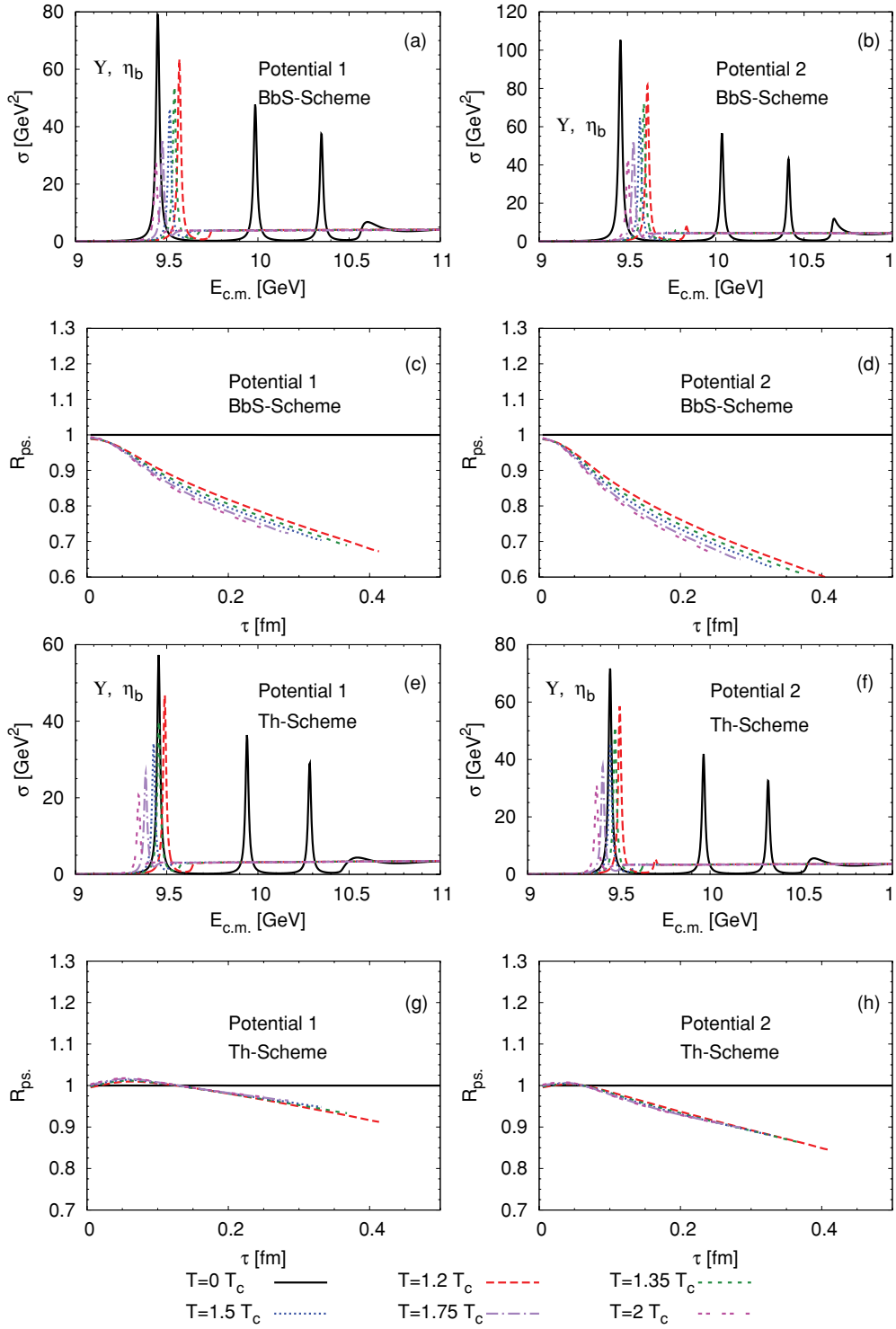

FIG. 17. (Color online) Same as in Fig. 15 but using F as potential.

broad "Feshbach resonances" (i.e., resonances at threshold) up to $\sim$1.5 T_c. Compared to previous T-matrix results [6], the diquark state is slightly more robust, due to the refined (color-blind) treatment of the string term (e.g., the ratio of peak heights for color antitriplet to color singlet at 1.2 T_c is about twice as large). For the charm-strange correlations similar patterns are found.

Next we calculate HQ relaxation rates. The original suggestion of nonperturbative effects in HQ diffusion has been put forward in Ref. [56] using an effective resonance model where the masses and coupling strengths were free parameters; within reasonable ranges of these, a factor 2–4 shorter thermalization times compared to pQCD were found. Subsequently, heavy-light T-matrix calculations [6] were carried out to render

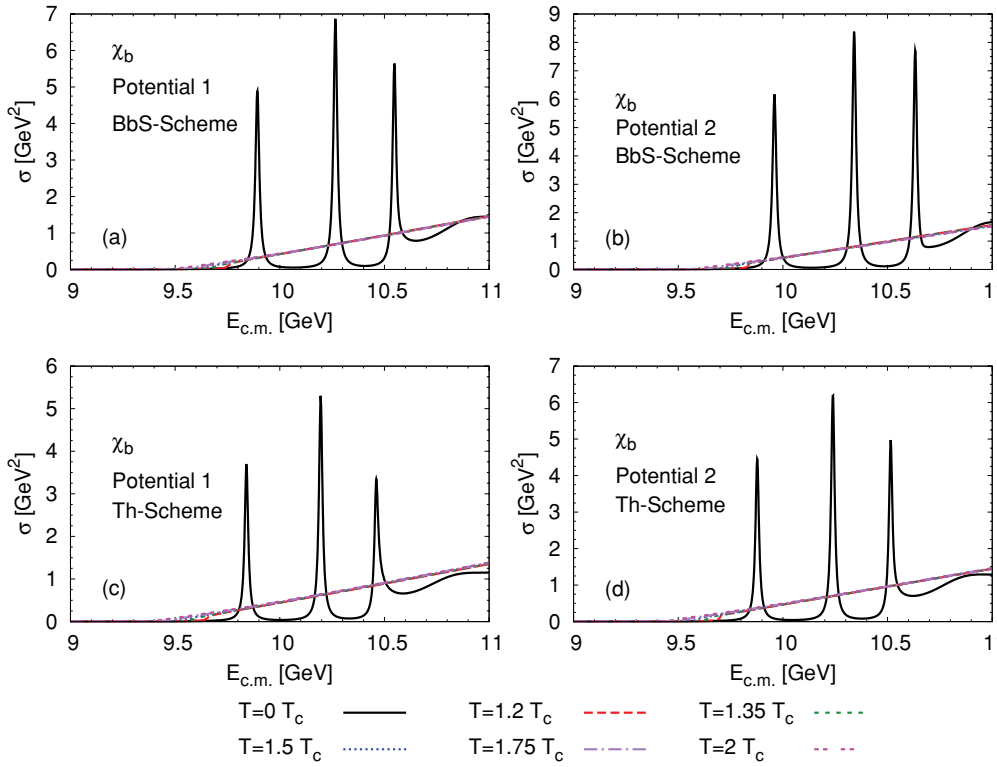

FIG. 18. (Color online) Same as in Fig. 16 but using F as potential.

the schematic estimates more quantitative (and to check for the existence of D-meson resonances in the QGP), roughly confirming the results of the resonance model *if* the U potential is employed. Here, we elaborate for the first time a quantitative connection to in-medium quarkonium properties. With the potential and all other parameters determined our relaxation rates, $A(p)$, are predictions of the approach. They are calculated utilizing Eq. (38) and displayed in Figs. 20 and 21 as a function of the HQ momentum for several temperatures above T_c. For completeness, we have added to the T-matrix results the contribution from HQ scattering off gluons using LO pQCD diagrams (including Debye screening) with a coupling constant $\alpha_s = 0.4$. At the lowest temperature, $T = 1.2\ T_c$, we find $\gamma_c = 0.14$–$0.2\ \text{fm}^{-1}$, where most of the variation is due to the potential choice while the reduction schemes agree within 10% for a given potential (pQCD scattering off gluons contributes, ca. $0.025\ \text{fm}^{-1}$). Thus, in the scattering regime the dependence on the reduction scheme is less pronounced than for bound states (see also Appendix A). The relaxation rate increases to 0.25–0.33 fm^{-1} at $2\ T_c$ (again with most of the spread owing to the difference in the potentials; pQCD scattering off gluons contributes, ca. $0.07\ \text{fm}^{-1}$). The magnitude of the low-momentum relaxation rates at $T = 1.2\ T_c$ ($2\ T_c$) is a factor 4–5 (2.5–3.5) larger than for a LO pQCD calculation for scattering off thermal quarks, antiquarks, and gluons with $\alpha_s = 0.4$. They are slightly larger than the previous T-matrix results of Ref. [6], where $\gamma_c = 0.12$–$0.19\ \text{fm}^{-1}$ has been obtained over the temperature range $T = 1.1$–$1.8\ T_c$ for parametrizations of yet two other (quenched [19,70] and $N_f = 2$ [37,71]) lQCD-based internal energies. In the previous calculations [6] a constant charm-quark mass of $m_c = 1.5$ GeV was used while we here include the in-medium self-energy from the infinite-distance limit of the internal (or free) energy. When using U, m_c^* is larger than 1.5 GeV up to temperatures of ca. $1.9\ T_c$ (potential-1 with Th scheme, see Table I and right panel of Fig. 3). The extra interaction strength in our present calculation compared to Ref. [6] is mostly due to the color-blind treatment of the string term, particularly in the diquark channel.

We emphasize that the in-medium HQ masses as used here are mandatory to maintain consistency with the quarkonium correlator ratios where they play a critical role in balancing the changes in binding energy. Our investigations actually show that the internal energy based on the quenched lQCD input from Refs. [19,70] leads to Euclidean correlator ratios for quarkonia which exhibit a large temperature variation (decrease with increasing T) incompatible with lQCD results, i.e., well beyond the 30% error margin deduced in Sec. IV B 1. The large temperature variation (screening) in the underlying potential leads to a *decrease* of the thermalization rate with temperature. This feature is not confirmed in the more quantitative calculations presented here. However, the increase with temperature of γ_c for our T-matrix (plus pQCD gluon scattering) calculations is significantly slower than for the LO pQCD calculations with temperature-dependent Debye mass: for $T = 1.2 \to 2T_c$ the former increase by a factor of $\sim$1.7 (less for the T-matrix contribution alone) compared to a factor of $\sim$2.5 for LO pQCD only (light anti-/quarks and gluons). Furthermore, in the T-matrix calculations $A(p)$ decreases appreciably with increasing three-momentum while the LO

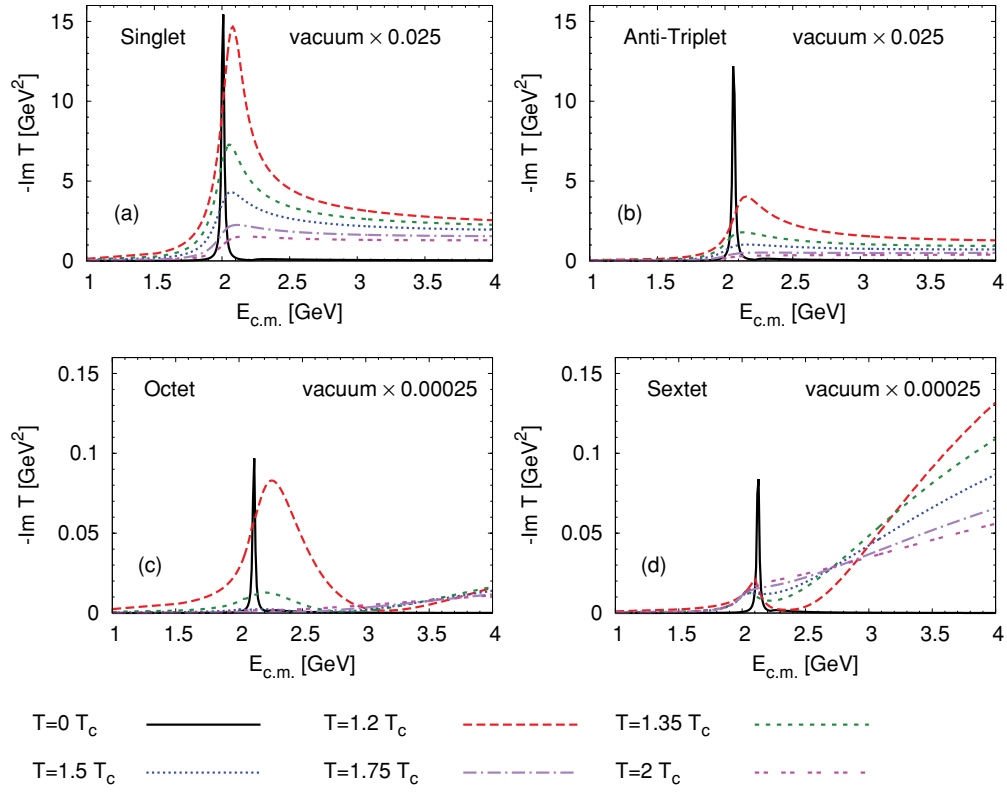

FIG. 19. (Color online) Imaginary part of the in-medium on-shell T matrix for charm-light quark scattering in the color-singlet (upper left), antitriplet (upper right), octet (lower left), and sextet (lower right) channels. In all cases lQCD potential-1 is used for U within the Thompson scheme. Note the factor 100 difference in the y scales of the upper and lower panels.

pQCD results are almost constant. This is simply due to the fact that with increasing three-momentum the charm quark is less likely to excite a low-energy Feshbach resonance in collisions with thermal quarks or antiquarks. At high three-momentum, resummation effects in the T matrix cease and the relaxation rates come closer to the LO pQCD results (recall the importance of the proper relativistic factors for this behavior). The difference at high three-momentum is mostly due to the smaller value of the screening mass of the Coulomb term in our lQCD fit relative to the pQCD value, $m_D^{\rm pQCD} = \sqrt{1+N_c/6}\, gT$. As in Ref. [6], the dominant contribution to the HQ relaxation rate originates from the S-wave meson (color-singlet) and diquark (color-triplet) channels, while the octet and sextet channels are suppressed (even at 1.2 T_c), as is immediately inferred from the magnitudes of the corresponding T matrices in Fig. 19. The P-wave channels contribute about 30% of the S waves.

When using F instead of U as potential the low-momentum charm-quark relaxation rate is reduced by approximately a factor of $\sim$2, but still larger by a factor of $\sim$2 than the LO pQCD results, cf. Fig. 21. Consequently, they come closer to the LO pQCD results at high momentum, even though a significant enhancement persists even at $p = 5$ GeV (mostly due to the differences in screening mass as mentioned above).

To put our results in context with other approaches we display in Fig. 22 (left panel) the temperature dependence of the relaxation rate at zero momentum for different models. Specifically, we compare our results for U and F to LO pQCD, to earlier T-matrix calculations [6] and to estimates from gravity-gauge duality (AdS/CFT) [72,73] (see also Refs. [74,75] for LO calculations with running coupling). The uncertainty bands associated with our T-matrix calculations are largely governed by the differences in the underlying lQCD input. As discussed above, the results using U overlap with the earlier T-matrix calculations (where also U has been used as potential), especially when the latter would be calculated with a color-blind string term. When using F the results are closer to, but still significantly above, LO pQCD. The AdS/CFT rates are markedly larger than any of the T-matrix rates, except for extrapolations close to T_c.

In the right panel of Fig. 22 we compile the temperature dependence of the spatial diffusion coefficients,

$$D_s = \frac{T}{m_c \gamma_c}, \tag{44}$$

for the above discussed approaches. We plot D_s in units of the thermal wavelength of the medium, $1/(2\pi T)$, which renders it suggestive for a connection to the widely discussed ratio of viscosity to entropy density; e.g., in kinetic theory for a weakly interacting gas one has the approximate relation

$$\frac{\eta}{s} \approx \frac{1}{5} T D_s. \tag{45}$$

In the strongly coupled limit of the AdS/CFT correspondence, one finds the same parametric dependence, albeit with a different numerical coefficient [the conjectured lower bound

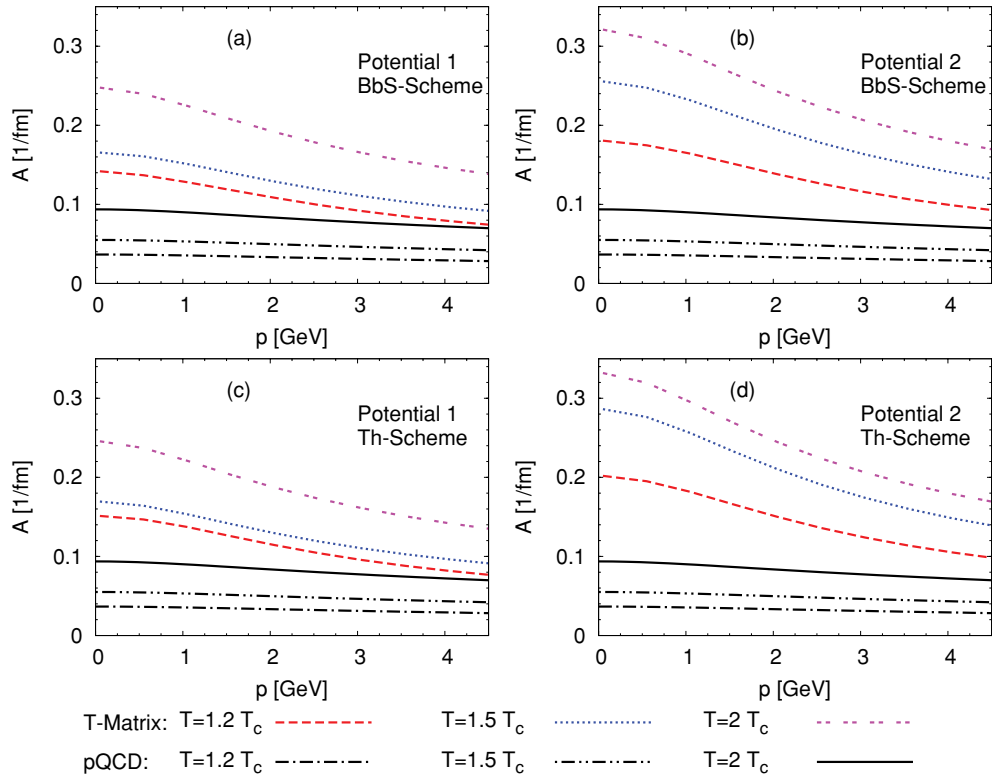

FIG. 20. (Color online) Charm-quark relaxation rate as a function of three-momentum calculated in the T-matrix approach using U as potential, compared the LO pQCD with $\alpha_s = 0.4$. A perturbative gluon contribution has been added to the heavy-light T-matrix rates.

of $\eta/s = 1/4\pi$ corresponds to diffusion at the thermal wavelength, $D_s \simeq 1/(2\pi\, T)$]. Besides the quantitative comparison of the D_s values their T dependence is of particular interest. It is constant for AdS/CFT [which has no scale other than temperature; note that the HQ mass is effectively divided out in Eq. (44)] and almost constant for LO pQCD and the T-matrix approach with F as potential, decreasing by less than 5% and up to 30%, respectively, for $T = 2 \to 1.2\ T_c$. The variation is larger, ca. 50%, if U is used as potential. The largest variation of more than 50% is found with the quenched lQCD input [19,70] for U in the previous T-matrix calculations, but, as we indicated above, this T dependence is incompatible with the small temperature variation in the Euclidean quarkonium correlator ratios. Nevertheless, our current, better constrained T-matrix calculations support a decreasing trend when approaching the "critical" temperature from above, as typical for many substances at or in the vicinity of a second-order transition.

In Figs. 23 and 24 we display the relaxation rates for bottom quarks for the U and F potentials, respectively. The general trends (and quantitative enhancements over LO pQCD) are very similar to the charm case so that an analogous discussion applies which we do not reiterate here.

V. SUMMARY AND CONCLUSIONS

We have set up a common framework to evaluate properties of open and hidden heavy-flavor states in the QGP. A thermodynamic T-matrix formalism for heavy quarkonia and heavy-light quark interactions has been combined with input potentials estimated from heavy-quark free energies computed in lattice QCD. Compared to earlier calculations, we have refined this link by utilizing a field-theoretic ansatz for an effective in-medium gluon propagator. This enabled the fits to be carried out at the level of the color-average free energy while disentangling color-Coulomb and confining interactions and thus gain insights into their medium modifications via the temperature dependence of the associated fit parameters (screening masses and coupling strengths). The T-matrix calculations further allowed us to identify appropriate relativistic corrections to the static potential, including differences between vector and scalar interactions for the color-Coulomb and confining parts, respectively; e.g., a color-Breit correction naturally emerges for the Coulomb term. The relativistic corrections are crucial to establish quantitative consistency for high-energy scattering between perturbative QCD and the T-matrix in the Born approximation. This connection is a prerequisite for a simultaneous treatment of bound and scattering states, which was one of the main objectives of our work.

The bare masses of the charm and bottom quark have been fixed to the (spin-averaged) mass of the quarkonium ground states, η_c-J/ψ and η_b-Υ, in vacuum. The resulting mass splittings for the excited states agree with the experimental values within ca. $\pm 10\%$, which is smaller than the effects due to hyperfine interactions which have been neglected in this work. The largest source of uncertainty turned out to be the static

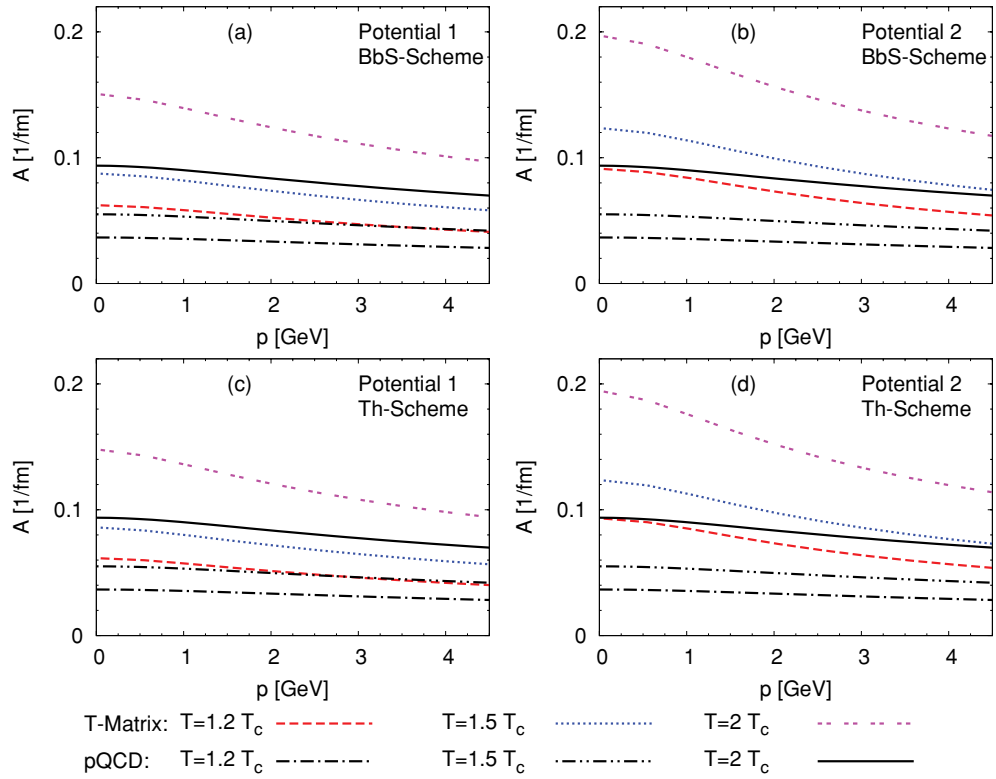

FIG. 21. (Color online) Same as in Fig. 20 but using F as potential.

reduction scheme underlying the scattering equation, while the two considered lattice potentials induced smaller variations. We also verified that the vacuum D- and B-meson masses are reasonably well recovered when using typical values for the constituent light- and strange-quark mass. As a by-product, we found that the scalar treatment of the confining force leads to shallow bound states in the color-sextet and -octet channels in vacuum, which might be relevant for a rather rich spectroscopy of narrow four-quark states as discussed in the recent literature.

Our finite-temperature calculations have been carried out within two scenarios of adopting an in-medium potential from the lattice results, either the free (F) or internal (U) energy. First, we calculated spectral functions and pertinent Euclidean-correlator ratios for heavy quarkonia. We confirmed the earlier found trend that for F charmonia dissolve rather close to T_c ($T_{\rm diss} \simeq 1.2\,T_c$) while for U the J/ψ may survive up to 2–2.5 T_c. However, both scenarios can lead to almost constant correlator ratios and thus to agreement with lattice QCD results for this quantity. The reason is a small in-medium

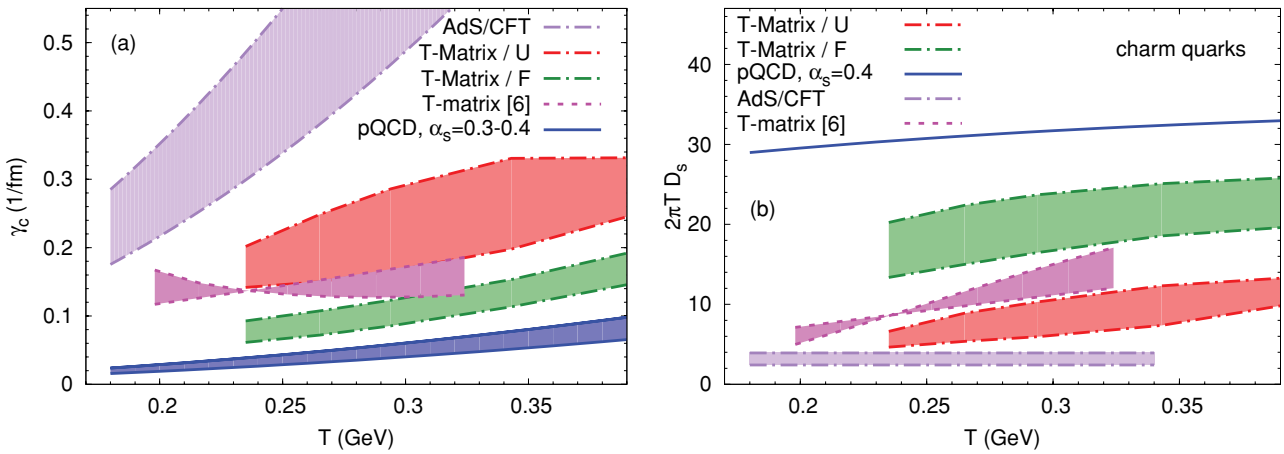

FIG. 22. (Color online) Comparison of our results for charm-quark relaxation rates (left plot) using U and F potentials to previous T-matrix calculations [6] and estimates from AdS/CFT [72,73]. The T-matrix rates have been augmented by perturbative scattering off thermal gluons. The right panel shows the corresponding spatial diffusion constants.

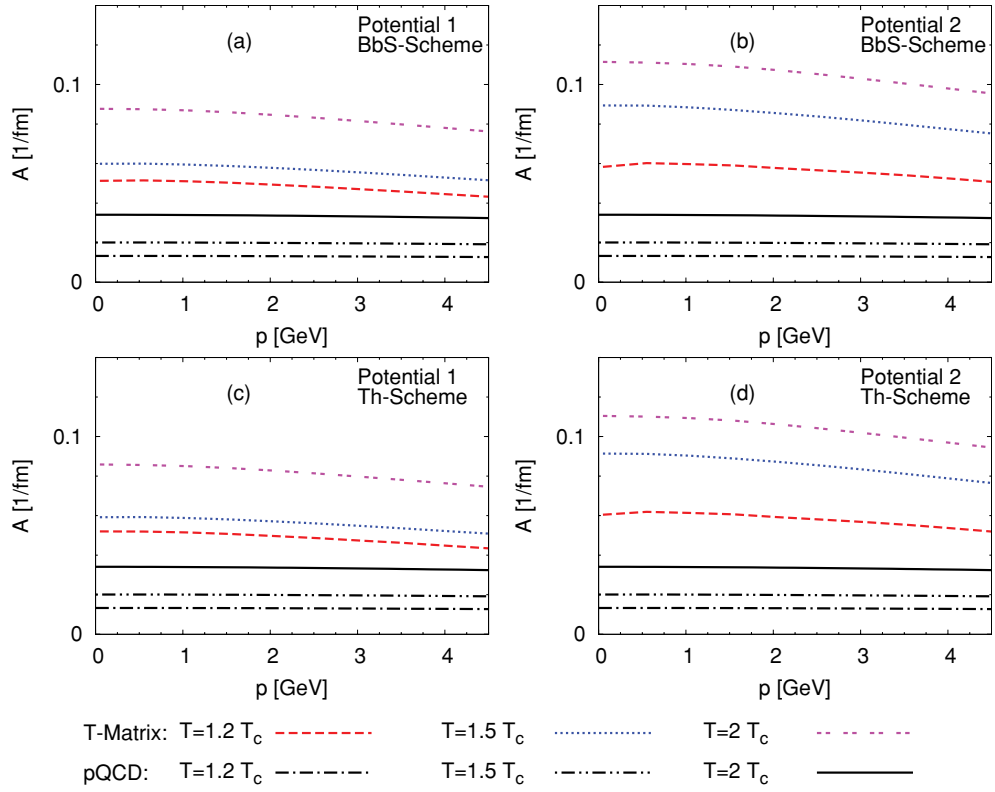

FIG. 23. (Color online) Bottom-quark relaxation rates as a function of three-momentum calculated in the T-matrix approach using U as potential (plus perturbative scattering off thermal gluons) compared to LO pQCD.

HQ mass correction when using F, while it is larger for U. As in the vacuum, we found significant variations due to the static reduction scheme, reflected by deviations of up to ∼40% in the correlator ratios at a given temperature. However, within a given reduction scheme, potential choice and lattice input, the relative *temperature* variation of the correlator ratios is usually much smaller. This suggests that future studies should scrutinize not only corrections to the static approximation but also the role of the reconstructed (vacuum) correlator figuring into the denominator of the ratios, especially close to threshold where hadronic ($D\bar{D}$) correlations could become important.

For heavy-flavor transport in the QGP, the use of U leads to a factor of ∼2 smaller thermalization times and (spatial) diffusion constant compared to F. This is largely due to "Feshbach"-type resonances in meson and diquark channels up to 1.3–1.5 T_c, but nonperturbative rescattering strength persists in the heavy-light T matrix for temperatures beyond 2 T_c. Even when using F as potential, these effects lead to up to a factor of 2 faster thermalization compared to perturbative scattering. The uncertainty due to the reduction scheme is smaller for heavy-quark transport coefficients than for quarkonium correlator ratios. The screening effects in the interaction generate a significant increase of the spatial diffusion constant (in units of the thermal wavelength) with temperature (especially for U), suggestive for a minimum toward T_c.

Our analyses suggest that a thermodynamic T-matrix approach can be used to establish quantitative relations between quarkonium survival and heavy-quark transport in the QGP. In particular, we have assessed uncertainties associated with commonly applied static (potential) and nonrelativistic approximations. While the latter are mandatory in the scattering regime, the former turned out to be on the few-tens-of-percentages level, which is relatively large for the lattice correlator ratios but relatively small in the context of current estimates for heavy-quark diffusion coefficients. A pressing issue remains the uncertainty in the definition of a finite-temperature potential, especially when based on model-independent input from thermal lattice QCD.

Several directions for future investigations emerge from our studies. As already mentioned, retardation effects and the influence of virtual antiparticle contributions need to be addressed, especially in the bound-state regime, e.g., by replacing the T matrix by a Dyson-Schwinger formalism at finite temperature. Such studies could also facilitate the treatment of heavy-quark interactions with thermal gluons beyond the perturbative level. A more microscopic treatment of the heavy-quark width figuring into the two-particle propagator of the scattering equation is desirable and in principle straightforward. Additional finite-width effects arise via inelastic interaction channels, which can be implemented via coupled channels into the T-matrix equation. For example, gluon radiation is expected to become important for high-energy charm-quark scattering and/or quarkonium dissolution, while $D\bar{D}$ or even magnetic charge-anticharge states could improve the description around T_c and extend it to temperatures below T_c. Heavy-quark susceptibilities, or

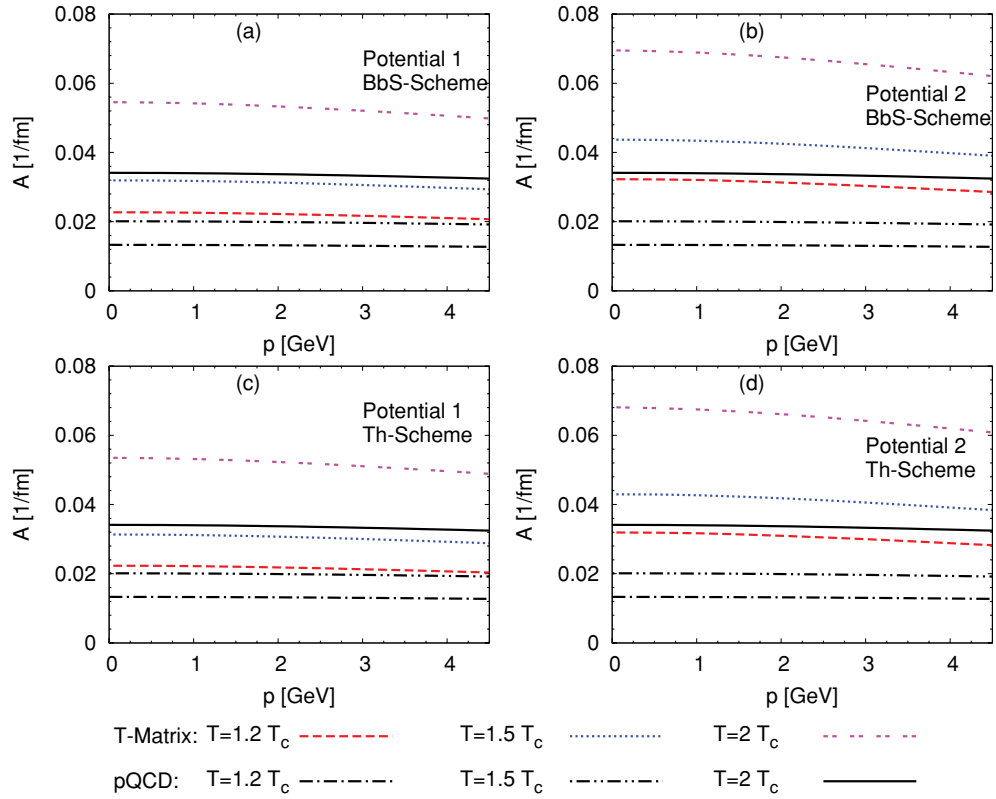

FIG. 24. (Color online) Same as in Fig. 23 but using F as potential.

more generally correlators of charm quarks with conserved charges (e.g., baryon or strangeness), which are computed with good accuracy in thermal lattice QCD, can be calculated with our T matrix. Here, the presence of broad resonances does not necessarily imply large signals in such quantities. The in-medium quarkonium and heavy-quark transport properties should be implemented into comprehensive phenomenological analyses of pertinent observables in heavy-ion collisions, e.g., via rate equations and/or Langevin simulations in a realistic bulk medium evolution. This will provide quantitative tests of the equilibrium results in current and future experiments and thus advance our understanding of strongly coupled QCD matter at temperatures around and above T_c. Work along some of these lines has been initiated.

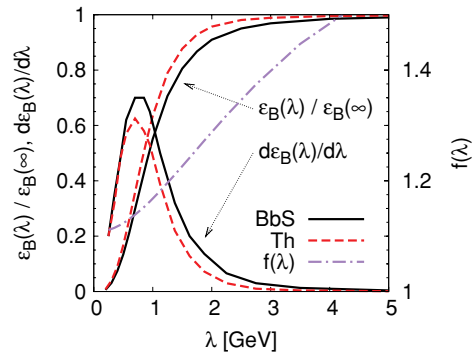

FIG. 25. (Color online) Dependence of the vacuum J/Ψ binding energy on a momentum cutoff introduced in the T-matrix integral in Eq. (15).

ACKNOWLEDGMENTS

We gratefully acknowledge discussions with D. Cabrera, H. van Hees, O. Kaczmarek, T.-S.H. Lee, R. Machleidt, M. Mannarelli, P. Petreczky, and A. Vairo on various aspects of this work. We especially thank O. Kaczmarek and P. Petreczky for providing their lattice QCD results. This work is supported by the U.S. NSF under Grants No. PHY-0449489 (CAREER) and No. PHY-0969394, and by the Alexander-von-Humboldt Foundation.

APPENDIX A: DIFFERENCES IN THE REDUCTION SCHEME

In this appendix we discuss differences between the BbS and Th reduction schemes. For this purpose we concentrate on the case of heavy quarkonium bound states. From Eqs. (16) it follows that the BbS and Th two-particle propagators differ as

$$G_{12}^{\mathrm{BbS}}(E,k) = \frac{4\,\omega_Q(k)}{E+2\,\omega_Q(k)}\, G_{12}^{\mathrm{Th}}(E,k) \qquad \text{(A1)}$$

due to a different treatment of the left-hand cut (virtual antiparticle contributions). Both reduction schemes should

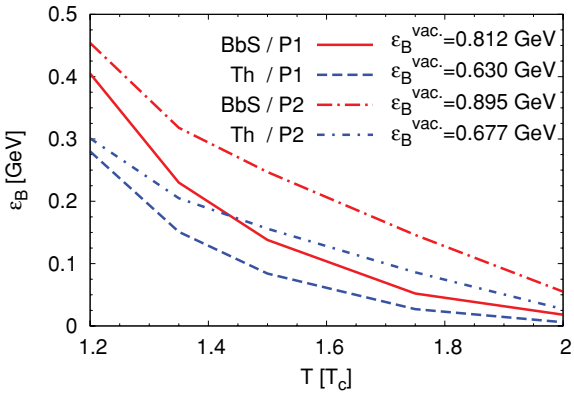

FIG. 26. (Color online) Temperature dependence of the binding energy (ϵ_B) of the J/Ψ (or η_c) using U as potential, for various combinations of reduction scheme and lQCD input.

give very similar results for the T-matrix if

$$f(k) = \frac{4\,\omega_Q(k)}{E + 2\,\omega_Q(k)} \approx 1. \tag{A2}$$

This condition is rather well satisfied in the scattering region, i.e., above the two-particle threshold, where the integral is dominated by the pole (unitarity cut) of the propagator, $E - 2\,\omega_Q(k) \approx 0$, which implies $E \approx 2\,\omega_Q(k)$. However, in the bound-state regime, i.e., below threshold, the situation can differ. For example, in the extreme case of $E \to 0$ the difference between the propagators becomes as large as a factor of 2, entailing large discrepancies in the results for the T-matrix. Let us try to asses the differences more quantitatively for the case at hand, i.e., for the binding energy of the charmonium ground state in vacuum. Our results for the BbS and Th scheme show a ca. 25% difference in the J/Ψ binding energy (the explicit values are quoted in the legend of Fig. 26). As a rough guideline, the influence of G on the binding may be estimated by formally writing the solution of the T matrix as $T = V/(1 - GV)$. At the bound-state energy, one has $GV = 1$, and thus a 25% change in G approximately "mimics" a 25% stronger potential or binding energy (for the same static input potential). Thus, for the BbS propagator in the T matrix integral one should expect, on average,

$$f(k) = \frac{4\,\omega_Q(k)}{E + 2\,\omega_Q(k)} \approx 1.25. \tag{A3}$$

To estimate the relevance of the integration momenta we apply a cutoff, λ, in the T-matrix equation (15) and study the dependence of $f(\lambda)$ and the J/ψ binding energy on this cutoff, as displayed in Fig. 25. Taking as an approximative representative momentum the one by which half of the binding is built up ($\lambda \simeq 1$ GeV) and evaluating the "BbS factor" at this value, one finds $f(\lambda) \simeq 1.2$. The magnitude of the deviations between BbS and Th for bound states can thus be roughly accounted for and is expected to become larger with increasing ratio of binding energy to the mass of the constituents.

APPENDIX B: BINDING ENERGIES

In this appendix we compile the temperature dependence of the binding energies of the J/ψ and Υ ground states. We define the binding energy as the difference between the quark-antiquark threshold, $2m_Q$, and the mass of the state in question. In the vacuum the J/ψ (η_c) binding energy is about 0.65(0.85) GeV for the Th (BbS) scheme. The in-medium binding energies are shown in Fig. 26 when using U as potential (for F the state already dissolves at about 1.3 T_c). One observes that the BbS scheme leads to a steeper dependence of the binding on temperature compared to the Th scheme while the melting temperature is quite similar in both cases.

A similar pattern occurs for the Υ ground state, displayed in the left and right panels of Fig. 27 when using U and F, respectively. Note, however, that the scheme dependence of the binding energy is significantly reduced in the bottomonium case, to about 10%, reflecting a better accuracy of the static approximation due to the larger bottom-quark mass, as expected. With the weaker interaction implicit in F the binding

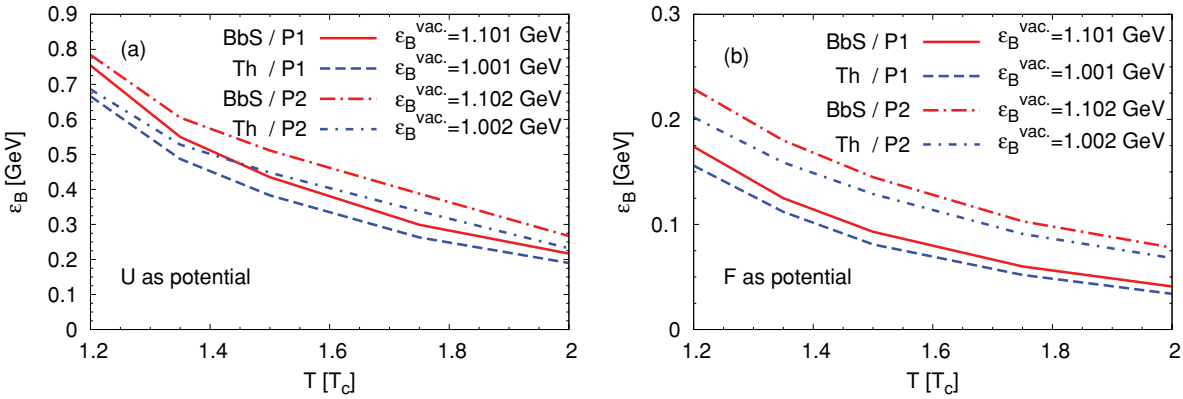

FIG. 27. (Color online) Temperature dependence of the binding energy (ϵ_B) of the Υ (or η_b) using U as potential (left plot) and F as potential (right plot) for various combinations of reduction scheme and lQCD input.

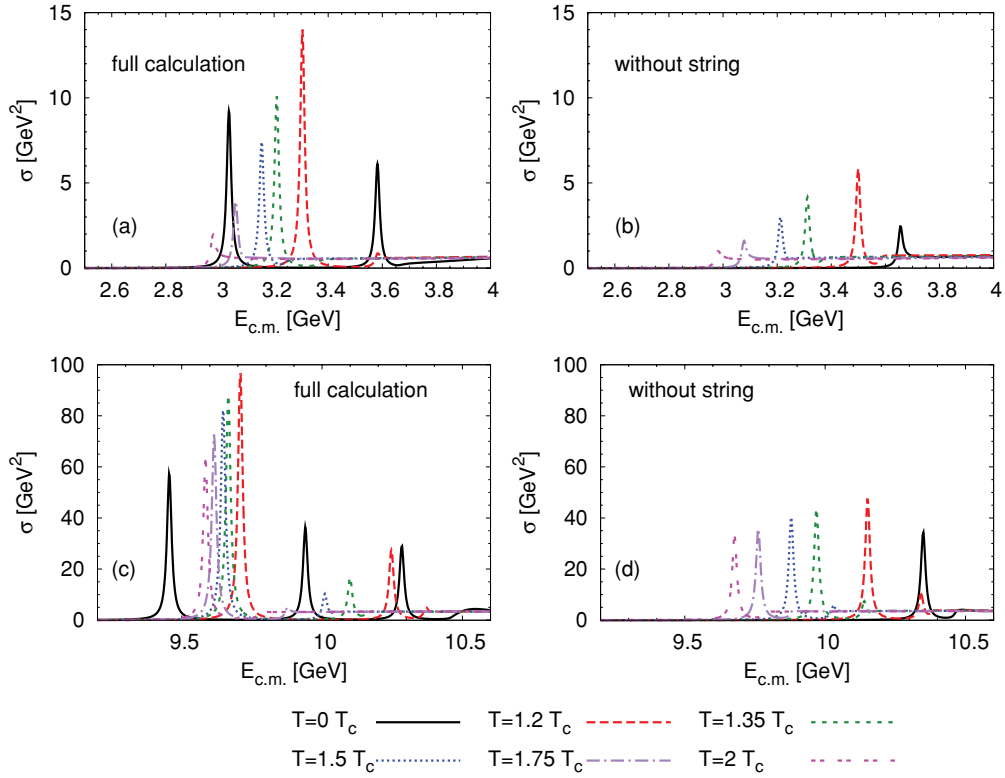

FIG. 28. (Color online) Comparison of the pseudoscalar spectral functions for charmonium (upper panels) and bottomonium (lower panels) using the full potential (left column) and the color-Coulomb term only (right column). In all cases U has been used as potential together with the Th reduction.

is reduced by about a factor of 4. The uncertainty induced by the different lQCD inputs is significantly larger than the one caused by the reduction scheme.

APPENDIX C: INFLUENCE OF THE CONFINING FORCE

In this appendix we assess the relevance of the confining interaction for bound-state formation. Recalling the definition of the free energy from Eq. (7),

$$F_a(r,T) = V_a^C(r,T) + V^S(r,T) + 2\Sigma_Q(T),$$

we repeat our calculations with the string term, V^S, switched off while all other parameters are kept fixed. The corresponding results for the internal energy, U, are obtained using Eq. (10) with the modified free energy (we keep, however, the self-energy from the full calculation). The results using U as the potential are presented in Fig. 28 using the Thompson reduction. For J/ψ (η_c) states the most striking difference occurs in the vacuum where without the confining interaction no excited bound states are supported and only a modest threshold enhancement remains for the ground state. In the medium the relevance of the string term gradually decreases until the results become similar to the full calculation for a temperature close to 2 T_c (even though the peak height is still smaller). This follows from the significantly stronger screening of the confining relative to the Coulomb term [$\tilde{m}_D(T)$ is much larger than $m_D(T)$ above T_c, recall Fig. 2]. Close to T_c half of the binding of the J/ψ is still supplied by remnants of the confining force. These systematics suggest that charmonia are rather sensitive to medium effects on the confining force in the temperature regime of 1–2 T_c. At first glance it might be surprising that the calculation without string term produces more binding in the medium than in the vacuum. The reason is that, without the string term, the internal energy, as given by Eq. (10), leads to a more attractive potential in the medium (up to $\sim$1.5 T_c) than in the vacuum (note that we are still using the large effective mass which, of course, is generated by the large-distance limit of the string term).

For the more tightly bound bottomonia (Υ) the sensitivity to the string term is still appreciable. In the vacuum the ground state is only bound by ca. 100 MeV while the excited states are unbound. In the medium a similar trend as in the charmonium sector is observed in that the significance of the string term ceases as temperature increases.

Generally, our findings clearly demonstrate the importance of the confining interaction in both charmonium and bottomonium spectroscopy, both in vacuum and in medium for temperatures of up to ca. 2 T_c. The use of potentials developed in a perturbative expansion therefore omits important physics in the description of quarkonium melting in medium.

[1] N. Brambilla *et al.* (Quarkonium Working Group), CERN Yellow Report No. CERN-2005-005, 2005.
[2] L. Kluberg and H. Satz, in *Relativistic Heavy-Ion Collisions*, edited by R. Stock and Landolt-Börnstein (Springer), New Series **I/23-A** (2010) 6-1; arXiv:0901.3831 [hep-ph].
[3] R. Rapp, D. Blaschke, and P. Crochet, Prog. Part. Nucl. Phys. (2010) doi:10.1016/j.ppnp.2010.07.002, arXiv:0807.2470 [hep-ph].
[4] P. Braun-Munzinger and J. Stachel, arXiv:0901.2500 [nucl-th].
[5] R. Rapp and H. van Hees, in *Quark-Gluon Plasma 4*, edited by R. Hwa and X. N. Wang (World Scientific, Singapore, 2010), arXiv:0903.1096 [hep-ph].
[6] H. van Hees, M. Mannarelli, V. Greco, and R. Rapp, Phys. Rev. Lett. **100**, 192301 (2008).
[7] D. Cabrera and R. Rapp, Phys. Rev. D **76**, 114506 (2007).
[8] M. Mannarelli and R. Rapp, Phys. Rev. C **72**, 064905 (2005).
[9] N. Brambilla, J. Ghiglieri, A. Vairo, and P. Petreczky, Phys. Rev. D **78**, 014017 (2008).
[10] M. Laine, O. Philipsen, P. Romatschke, and M. Tassler, J. High Energy Phys. 03 (2007) 054.
[11] A. Beraudo, J. P. Blaizot, and C. Ratti, Nucl. Phys. A **806**, 312 (2008).
[12] O. Kaczmarek, PoS **CPOD07**, (2007) 043.
[13] P. Petreczky and K. Petrov, Phys. Rev. D **70**, 054503 (2004).
[14] O. Kaczmarek and F. Zantow, Phys. Rev. D **71**, 114510 (2005).
[15] A. Mocsy and P. Petreczky, Phys. Rev. D **73**, 074007 (2006).
[16] C. Y. Wong and H. W. Crater, Phys. Rev. D **75**, 034505 (2007).
[17] W. M. Alberico, A. Beraudo, A. De Pace, and A. Molinari, Phys. Rev. D **75**, 074009 (2007).
[18] A. Dumitru, Y. Guo, A. Mocsy, and M. Strickland, Phys. Rev. D **79**, 054019 (2009).
[19] C.-Y. Wong, Phys. Rev. C **72**, 034906 (2005).
[20] O. Philipsen, Nucl. Phys. A **820**, 33c (2009).
[21] E. Megias, E. R. Arriola, and L. L. Salcedo, Phys. Rev. D **75**, 105019 (2007).
[22] E. Megias, E. Ruiz Arriola, and L. L. Salcedo, J. High Energy Phys. 01 (2006) 073.
[23] G. E. Brown, Philos. Mag. **43**, 467 (1952).
[24] M. J. Lavelle and M. Schaden, Phys. Lett. B **208**, 297 (1988).
[25] F. V. Gubarev and V. I. Zakharov, Phys. Lett. B **501**, 28 (2001).
[26] F. V. Gubarev, L. Stodolsky, and V. I. Zakharov, Phys. Rev. Lett. **86**, 2220 (2001).
[27] K.-I. Kondo, Phys. Lett. B **514**, 335 (2001).
[28] D. Dudal, Phys. Lett. B **677**, 203 (2009).
[29] P. Boucaud *et al.*, Phys. Lett. B **493**, 315 (2000).
[30] P. Petreczky, Eur. Phys. J. C **43**, 51 (2005).
[31] O. Kaczmarek, F. Karsch, P. Petreczky, and F. Zantow, Phys. Lett. B **543**, 41 (2002).
[32] M. Doring, K. Hubner, O. Kaczmarek, and F. Karsch, Phys. Rev. D **75**, 054504 (2007).
[33] S. Digal, S. Fortunato, and P. Petreczky, Phys. Rev. D **68**, 034008 (2003).
[34] F. Zantow, O. Kaczmarek, F. Karsch, and P. Petreczky, Proceedings of SEWM 2002 (Heidelberg, 2–5 October 2002), arXiv:hep-lat/0301015.
[35] A. Nakamura and T. Saito, Phys. Lett. B **621**, 171 (2005).
[36] H. Satz, J. Phys. G **36**, 064011 (2009).
[37] E. V. Shuryak and I. Zahed, Phys. Rev. D **70**, 054507 (2004).
[38] A. Rothkopf, T. Hatsuda, and S. Sasaki, Proceedings of LATTICE 2009 (Beijing, 25–31 July 2009), arXiv:0910.2321 [hep-lat].
[39] O. Kaczmarek (private comunications).
[40] M. Cheng *et al.*, Phys. Rev. D **77**, 014511 (2008).
[41] P. Petreczky (private comunications).
[42] R. Blankenbecler and R. Sugar, Phys. Rev. **142**, 1051 (1966).
[43] R. H. Thompson, Phys. Rev. D **1**, 110 (1970).
[44] R. Machleidt, Adv. Nucl. Phys. **19**, 189 (1989).
[45] A. Vairo (private comunications).
[46] N. Brambilla, D. Gromes, and A. Vairo, Phys. Lett. B **576**, 314 (2003).
[47] J. Fröhlich, K. Schwarz, and H. F. K. Zingl, Phys. Rev. C **27**, 265 (1983).
[48] R. J. Yaes, Phys. Rev. D **3**, 3086 (1971).
[49] M. Haftel and F. Tabakin, Nucl. Phys. A **158**, 1 (1970).
[50] G. E. Brown, C.-H. Lee, M. Rho, and E. Shuryak, Nucl. Phys. A **740**, 171 (2004).
[51] T. Umeda, Phys. Rev. D **75**, 094502 (2007).
[52] G. Aarts and J. M. Martinez Resco, Nucl. Phys. B **726**, 93 (2005).
[53] P. Petreczky and D. Teaney, Phys. Rev. D **73**, 014508 (2006).
[54] B. Svetitsky, Phys. Rev. D **37**, 2484 (1988).
[55] V. Herrmann and K. Nakayama, Phys. Rev. C **46**, 2199 (1992).
[56] H. van Hees and R. Rapp, Phys. Rev. C **71**, 034907 (2005).
[57] M. Cheng *et al.*, Phys. Rev. D **81**, 054504 (2010).
[58] C. Amsler *et al.* (Particle Data Group), Phys. Lett. B **667**, 1 (2008).
[59] L. Maiani, F. Piccinini, A. D. Polosa, and V. Riquer, Phys. Rev. D **71**, 014028 (2005).
[60] L. Maiani, V. Riquer, F. Piccinini, and A. D. Polosa, Phys. Rev. D **72**, 031502 (2005).
[61] D. Ebert, R. N. Faustov, and V. O. Galkin, Eur. Phys. J. C **58**, 399 (2008).
[62] A. Jakovac, P. Petreczky, K. Petrov, and A. Velytsky, Phys. Rev. D **75**, 014506 (2007).
[63] G. Aarts, C. Allton, M. B. Oktay, M. Peardon, and J. I. Skullerud, Phys. Rev. D **76**, 094513 (2007).
[64] A. Mocsy and P. Petreczky, Phys. Rev. D **77**, 014501 (2008).
[65] S. Datta, F. Karsch, P. Petreczky, and I. Wetzorke, Phys. Rev. D **69**, 094507 (2004).
[66] A. Beraudo, J. P. Blaizot, G. Garberoglio, and P. Faccioli, Nucl. Phys. A **830**, 319c (2009).
[67] M. Le Bellac, *Thermal Field Theory* (Cambridge University Press, New York, 2000).
[68] P. Levai and U. W. Heinz, Phys. Rev. C **57**, 1879 (1998).
[69] A. Peshier, B. Kampfer, and G. Soff, Phys. Rev. D **66**, 094003 (2002).
[70] O. Kaczmarek, F. Karsch, P. Petreczky, and F. Zantow, Nucl. Phys. Proc. Suppl. **129**, 560 (2004).
[71] O. Kaczmarek *et al.*, Prog. Theor. Phys. Suppl. **153**, 287 (2004).
[72] Y. Akamatsu, T. Hatsuda, and T. Hirano, Phys. Rev. C **79**, 054907 (2009).
[73] S. S. Gubser, Phys. Rev. D **76**, 126003 (2007).
[74] A. Peshier, arXiv:0801.0595 [hep-ph].
[75] P. B. Gossiaux and J. Aichelin, Phys. Rev. C **78**, 014904 (2008).